Sorption of beryllium in cementitious systems relevant for nuclear waste disposal: Quantitative description and mechanistic understanding

N. Cevirim-Papaioannou[1,*], I. Androniuk[1], S. Han[2], N. Ait Mouheb[1,a], S. Gaboreau[3], W. Um[2], X. Gaona[1,*], M. Altmaier[1]

[1]*Institute for Nuclear Waste Disposal (INE), Karlsruhe Institute of Technology (KIT), Karlsruhe, Germany*

[2]*Division of Advanced Nuclear Engineering (DANE), Pohang University of Science and Technology (POSTECH), Pohang, Gyeongbuk, South Korea*

[3]*BRGM Bureau de Recherches Géologiques et Minières, Orleans, France*

*corresponding authors.

E-mail addresses: nese.cevirim@kit.edu (N. Cevirim-Papaioannou), xavier.gaona@kit.edu (X. Gaona)

[a]Current address: Forschungszentrum Jülich GmbH, Institute of Energy and Climate Research – Nuclear Waste Management and Reactor Safety (IEK-6), Jülich, Germany

Abstract

Beryllium has applications in fission and fusion reactors, and it is present in specific streams of radioactive waste. Accordingly, the environmental mobility of beryllium needs to be assessed in the context of repositories for nuclear waste. Although cement is widely used in these facilities, Be(II) uptake by cementitious materials was not previously investigated and was hence assumed negligible.

Sorption experiments were performed under Ar-atmosphere. Ordinary Portland cement, low pH cement, calcium silicate hydrated (C–S–H) phases and the model system TiO_2 were investigated. Sorption kinetics, sorption isotherms and distribution ratios (R_d, in $kg \cdot L^{-1}$) were determined for these systems. Molecular dynamics were used to characterize the surface processes driving Be(II) uptake.

A strong uptake ($5 \leq \log Rd \leq 7$) is quantified for all investigated cementitious systems. Linear sorption isotherms are observed over three orders of magnitude in [Be(II)]aq, confirming that the uptake is controlled by sorption processes and that solubility phenomena is not relevant within the investigated conditions. The analogous behaviour observed for cement and C–S–H support that the latter are the main sink of beryllium. The two step sorption kinetics is explained by a fast surface complexation process, followed by the slow incorporation of Be(II) in C–S–H. Molecular dynamics indicate that $Be(OH)_3^-$ and $Be(OH)_4^{2-}$ are sorbed to the C–S–H surface through Ca-bridges.

This work provides a comprehensive quantitative and mechanistic description of Be(II) uptake by cementitious materials, whose retention properties can be now reliably assessed for a wide range of boundary conditions of relevance in nuclear waste disposal.

Keywords: *beryllium, sorption, cement, C-S-H phases, molecular dynamics, mechanistic understanding*

1. Introduction

Beryllium is used as neutron reflector and moderator in test and research fission reactors due to its specific chemical and structural properties, relatively low neutron absorption cross section and high neutron scattering cross section (Beeston 1970; Longhurst et al. 2003; Chandler et al. 2009). Beryllium is also considered as a plasma-facing material and neutron multiplication in breeding blankets in fusion reactors (Longhurst et al. 2003; Kawamura et al. 2004). In these applications, substantial amounts of ^{4}He, ^{3}He and ^{3}H gases are generated as a result of (n, 2n) and (n, α) reactions, leading to the swelling of beryllium and to significant changes in its mechanical properties (Chandler et al. 2009; Longhurst et al. 2003). Irradiated beryllium components must be regularly replaced, and thus are part of the inventory in specific wastestreams of nuclear waste.

Deep underground repositories are considered in several countries for the final disposal of radioactive waste. The safety concept in such repositories relies on the combination of engineered and geological barriers, which minimize the release of radionuclides into the biosphere. Cementitious materials are used for the stabilization of the waste and for construction purposes, mostly (but not exclusively) in the case of low- and intermediate level radioactive waste (L/ILW). The contact of cement with groundwater leads to its chemical degradation, which is commonly described in three degradation stages (Atkinson et al. 1988; Berner 1992; Wieland and Van Loon 2003; Ochs et al. 2016; Tits and Wieland 2018). In the first degradation stage, the composition of the porewater is controlled by the dissolution of K- and Na-oxide/hydroxides, buffering the pH at ≈ 13.3 and leading to high alkali concentrations in solution ($[K^+] \approx 0.18$ M, $[Na^+] \approx 0.11$ M). Degradation stage II is dominated by the dissolution of portlandite, $Ca(OH)_2$, which buffers the pH at ≈ 12.5 and imposes high calcium concentrations in the pore water ($[Ca]_{tot} \approx 2 \cdot 10^{-2}$ M). After the complete dissolution of portlandite, the third degradation stage is characterized by the incongruent dissolution of calcium silicate hydrated (C-S-H) phases. Throughout this process, the Ca:Si ratio of C-S-H phases varies from ≈ 1.6 to ≈ 0.6, whilst the pH decreases from ≈ 12.5 to ≈ 10.

Low-pH cement formulations are gaining relevance in the context of nuclear waste disposal due to the negative impact that high-pH plumes can potentially have on other natural or engineered barriers, especially those containing clay materials. In low-pH cements, discussed for potential use in order to limit alkalinity inventories, the addition of materials such as silica fume, blast furnace slag or fly ash to cement results in a low content / absence of portlandite and an increased fraction of C-S-H phases with low Ca:Si ratio (Coumes et al. 2006; Savage

and Benbow 2007; Codina et al. 2008; Calvo et al. 2010; Lothenbach et al. 2012; Vasconcelos et al. 2020).

C-S-H phases are considered as the main sink of several metal ions in cementitious materials. Three main mechanisms are described in the literature for the uptake of metal ions by C-S-H phases: (i) surface complexation onto the silanol groups of the C-S-H surface, (ii) incorporation in C-S-H structure by replacement of Ca^{2+} in the CaO layers, and (iii) development of a bond to the interlayer silandiol groups, which can be also interpreted as incorporation in the C-S-H interlayer (Tits and Wieland 2018).

In contrast to beryllium, the uptake of other alkali-earth metals by cementitious materials has been extensively investigated in the literature (Bayliss et al. 1989; Holland and Lee 1992; Tits et al. 2006a; Tits et al. 2006b; Wieland et al. 2008; Dauzeres et al. 2010; Jenni et al. 2014; Lothenbach et al. 2015; Missana et al. 2017; Olmeda et al. 2019). Sr(II), Ba(II) and Ra(II) are characterized by a weak to moderate uptake, with R_d values ranging from 10 to 10^4 $L \cdot kg^{-1}$. Both surface complexation and ion exchange with Ca are described as main uptake mechanisms for these metals. On the other hand, Mg(II) is known to form magnesium silicate hydrated phases (M-S-H), which are stable in alkaline systems with pH ≈ 8 to ≈ 11 (Dauzeres et al. 2010; Jenni et al. 2014; Lothenbach et al. 2015).

A number of experimental studies available in the literature have investigated the uptake of other divalent metals (*e.g.* Fe(II), Zn(II), Cd(II), Pb(II), among others) by cement and C-S-H phases (Ziegler et al. 2001a; Pomies et al. 2001; Pointeau et al. 2001a; Ziegler et al. 2001b; Ochs et al. 2002; Tommaseo and Kersten 2002; Mancini et al. 2020). For some of these elements (*e.g.* Zn(II), Pb(II)), the uptake by cement and C-S-H phases has been reported to decrease with increasing pH. The analogies in the aqueous speciation of these metal ions with Be(II), which involve the predominance of $M(OH)_3^-$ and $M(OH)_4^{2-}$ hydrolysis species in hyperalkaline systems, may provide relevant insights to understand the uptake of beryllium by cementitious materials.

Aluminium is a relevant element in cementitious systems, where it is predominantly found as calcium aluminate hydrate phases (AFm) and ettringite (Taylor 1997). Aluminium is taken up strongly by C-S-H phases, and has been reported to form Al-substituted C-S-H phases (L'Hopital et al. 2015; Barzgar et al. 2020). Due to the similar z/d ratio and aqueous speciation in hyperalkaline systems, aluminum has been proposed as possible chemical analogue to assess the uptake of beryllium by cementitious materials (Ochs et al. 2016).

Molecular modelling allows interpretation of the experimentally observed interfacial behaviour on the atomic and molecular scale considering the effects of the structure and composition of the surface on the interaction. C-S-H interfaces are complex systems with disordered structures (Grangeon et al. 2017; Monteiro et al. 2019), and larger system sizes and longer simulation times, compared to routine quantum simulation set-ups, are therefore required to obtain meaningful statistical data to describe sorption processes (Mutisya et al. 2017). Quantum chemical calculations are more precise, but they are computationally very expensive, and thus mostly used either to describe preselected sorption sites on the surface, and incorporated species, where ion mobility is less important (Kremleva et al. 2020; Lange et al. 2018), or to study substitution reactions with simpler and smaller systems (Churakov and Labbez 2017). When sorption sites are not known, molecular dynamics (MD) simulations are typically used to study sorption mechanisms of ions on cementitious materials (Honorio et al. 2019; Bu et al. 2019; Androniuk and Kalinichev 2020), and this method was chosen to study the sorption of beryllium on the C-S-H surface.

Many computational studies have been previously conducted to describe the behaviour of beryllium complexes in aqueous solutions on a molecular scale, and significant efforts have been dedicated to go beyond the classical two-body potentials for aqueous Be^{2+} ions to describe its interactions realistically using molecular dynamics (D'Incal et al. 2006; Gnanakaran et al. 2008; Azam et al. 2009; Raymond et al. 2020). The 12-6-4 Lennard-Jones-type nonbonded parameters for Be^{2+} and Ca^{2+} have been used in our simulations. This model can reproduce the correct geometry for the binding of cations as observed in crystal structures, and the experimental hydration free energies (De et al. 2020; Li and Merz 2014; Li et al. 2020). Combinational analysis of the time-averaged local structures and 1D and 2D density profiles for target aqueous species together with the experimental data provides an insight into the prevailing uptake mechanisms and the preferential sorption sites on the surface.

In the context of the EU funded collaborative project "Cement-based materials, properties, evolution, barrier functions" (Cebama), the present study aims at a comprehensive investigation of beryllium uptake by cementitious systems. The cement materials investigated include an ordinary Portland cement in the degradation stage II, a low pH cement defined as the *Cebama reference cement* (Vehmas et al. 2020), as well as C-S-H phases with Ca:Si = 0.6, 1.0 and 1.6. The latter phases are expectedly the main sink of Be(II) in cement. Sorption experiments with TiO_2 are performed to gain additional insight on the mechanisms driving the uptake of Be(II) in hyperalkaline systems. Surface complexation is known to be the main uptake mechanism in

TiO_2 systems (Bouby et al. 2010; Tits et al. 2011; Tits et al. 2014; Tits et al. 2015), thus allowing to distinguish the possible incorporation mechanism into the C-S-H phases. Beyond the quantitative investigation of the uptake on the basis of sorption kinetics, sorption isotherms and distribution ratios, the use of molecular dynamics provides a very accurate description of the surface processes driving the uptake of beryllium at molecular scale. This work complements and further extends our previous study on the solubility, hydrolysis and thermodynamic description of Be(II) in alkaline to hyperalkaline conditions relevant for cementitious systems (Cevirim-Papaioannou et al. 2020).

2. Experimental

2.1. Chemicals and analytical methods

All solutions and samples were prepared with purified water (Milli–Q academic, Millipore, 18.2 MΩ·cm) purged with Ar for at least one hour before use to remove CO_2(g) dissolved in solution. Sample preparation, handling and equilibration were performed in an Ar–glove box (O_2 < 1 ppm) at T = (22 ± 2) ºC. $BeSO_4{\cdot}4H_2O$ (99.99%), NaCl EMSURE, KCl EMSURE, NaOH Titrisol, KOH Titrisol and HCl Titrisol were obtained from Merck. CaO, Na_2SO_4, $Na_2O_7Si_3$, $CaCl_2{\cdot}H_2O$, $CaCO_3$ and $Ca(OH)_2$, H_2SO_4 (96%) were all of analytical grade and were purchased from Merck. TiO_2 (Degussa P-25) and SiO_2 (AEROSIL 300) were obtained from Evonik Industries.

The pH in solution was measured using combination pH electrodes (ROSS Orion, with 3.0 M KCl as filling solution). Calibration of the electrode was performed with standard pH buffers (pH 1-12, Merck).

2.2. Sorption materials used in this study

A monolith of a hydrated cement paste (HCP, CEM I 42,5 N BV/SR/LA type) was provided by the Swedish Nuclear Fuel and Waste Management Company (SKB) in Sweden. The HCP was milled, sieved to a particle size of < 100 μm as described in Tasi *et al.* (2021) and stored under Ar atmosphere until use in the sorption experiments. An extensive characterization of the HCP

(XRD, TGA-DSC, XPS, BET) is provided in Tasi *et al.* (2021). The surface area of the powder material used in the present study was determined by Tasi and co-workers as 79.2 $m^2 \cdot g^{-1}$.

A monolith of the *CEBAMA reference cement* (low pH cement, CEM I 42.5 MH/SR/LA mixture with silica fume, BFS and plasticiser pantarhit) was provided by the Technical Research Centre of Finland (VTT) (Vasconcelos et al. 2020; Vehmas et al. 2020) within the CEBAMA project. All surfaces (≈ 5 mm thickness) of the cement monolith were cut under Ar atmosphere using a radial saw in order to remove the potentially carbonated surface. Afterwards, the cement block was crushed and powdered with a grinder, then sieved to a particle size of < 63µm and stored under Ar atmosphere. The characterization of the *CEBAMA reference cement* is reported in Vasconcelos *et al.* (2020). The latter authors reported a Ca:Si = (0.9 ± 0.1) for the hydrated material after a curing time of 18 months.

Boiled and degassed ultrapure water was used in the synthesis of C-S-H phases. All C-S-H phases were prepared by mixing $Ca(OH)_2$-Prolabo which was heated at 1000°C for 24 h and SiO_2 (Aerosil 200, Degussa) in inert atmosphere (N_2 glovebox). C-S-H phases with Ca:Si ratio ranging from 0.6 to 1.6 were precipitated at 22°C. Further details on the preparation and characterization of C-S-H phases are reported elsewhere (Gaboreau et al. 2020).

The commercial TiO_2 used in this work was extensively characterized by XRD, BET, photon correlation spectroscopy and FTIR in a previous study (Bouby et al., 2010). The authors reported a composition of 85% anatase and 15% rutile, with an average surface area of 50.6 $m^2 \cdot g^{-1}$. Bouby and co-workers determined also the point of zero charge (pzc) of this material as pH_{pzc} = 6.1. TiO_2 is a sparingly soluble metal oxide (Schmidt and Vogelsberger 2009), which has been extensively used in previous sorption studies covering acidic to hyperalkaline pH conditions (Bouby et al. 2010; Tits et al. 2011; Tits et al. 2014; Tits et al. 2015). TiO_2 is considered in this work as a reference material to assess the surface complexation behavior of Be(II) within the investigated pore water conditions.

2.3. Preparation of cement pore waters

Sorption experiments with HCP targeted the degradation stage II of cement. To obtain the corresponding pore water solution, the powdered HCP (≤ 100 µm) was immersed in 1 L of Milli-Q water at a solid to liquid ratio (S:L) of 25 $g \cdot L^{-1}$. This suspension was shaken regularly for two weeks under Ar atmosphere. Thereafter, the supernatant was removed and eventually, the same volume of Milli-Q water was contacted with the HCP to retain the same S:L ratio. The

resulting pore water is representative of the cement degradation stage II, *i.e.* low alkali content, pH ≈ 12.5 and $[Ca]_{tot} \approx 2 \cdot 10^{-2}$ M as buffered by portlandite.

The artificial pore water of the *CEBAMA reference cement* was prepared as described in Ait Mouheb et al. (2019). Corresponding amounts of KOH, CaO, Na_2SO_4, $Na_2O_7Si_3$, $CaCl_2 \cdot H_2O$, $CaCO_3$ and $Ca(OH)_2$ were dissolved in 660 mL of Milli-Q water, and the pH adjusted with a 0.04 M H_2SO_4 solution. The resulting pore water was filtered with membrane filter (0.2 μm, Millipore) before the preparation of the sorption samples.

Artificial pore water for C-S-H phases with Ca:Si = 0.6, 1.0 and 1.6 were prepared with Milli-Q water, CaO and SiO_2 targeting the pH, [Ca] and [Si] of the original C-S-H phases as reported in (Gaboreau et al. 2020).

Besides the investigated cementitious systems, the uptake of Be(II) by TiO_2 was studied in contact with the pore water solutions of C-S-H 1.0, C-S-H 1.6 and HCP in the degradation stage I. The latter system was considered to provide an upper pH limit in the sorption experiments with TiO_2. The corresponding artificial pore water was prepared as described in Han et al. (2021), and is characterized by pH values of ≈ 13.2, [Na] = 0.032 M, [K] = 0.075 M, [Ca] = $4.1 \cdot 10^{-4}$ M and [Si] = $1.1 \cdot 10^{-4}$ M.

2.4. Sorption experiments

All experiments were carried out under Ar atmosphere. The sorption samples with cement (HCP or low pH), C-S-H phases or TiO_2 were prepared with 20 mL of the corresponding pore water solution (see section 2.4) and a S:L = 0.2 or 2 $g \cdot L^{-1}$. $BeSO_4$ stock solutions (0.35 – 10^{-3} M) were used to obtain the targeted initial Be concentrations, *i.e.* $3 \cdot 10^{-3}$ M ≤ $[Be]_0$ ≤ 10^{-6} M. The range of Be concentration considered for each system was selected on the basis of the solubility data reported in Cevirim-Papaioannou et al. (2020) for α-$Be(OH)_2$. Table 1 summarizes the experimental boundary conditions considered for the sorption experiments.

Sorption samples with HCP (deg. stage II) and low pH cement were contacted with the corresponding pore water solutions. Stock suspensions (S:L = 4 $g \cdot L^{-1}$) of C-S-H phases with Ca:Si = 0.6, 1.0 and 1.6 were diluted with the artificial pore waters of each phase in order to obtain the targeted S:L = 2 $g \cdot L^{-1}$. Due to the strong uptake observed for this system, additional samples with S:L = 0.2 $g \cdot L^{-1}$ were prepared for C-S-H 0.6. The samples containing TiO_2 were prepared by contacting the solid material with pore waters of C-S-H 1.0 (pH = 12.1), C-S-H 1.6 (pH = 12.6) and HCP (degradation stage I, pH = 13.2), in all cases with S:L = 2 $g \cdot L^{-1}$.

***Table 1**. Experimental conditions considered in the uptake experiments with Be(II), cementitious materials and TiO_2. p.w. refers to the cementitious pore waters used in the experiments with TiO_2.*

Sorbent		S/L [g·L^{-1}]	Eq. time (d)	pH	Initial [Be] [M]	Number of samples
C-S-H phases	Ca:Si = 0.6	0.2, 2	4-145	10.1	$3\cdot10^{-6}$-$1\cdot10^{-3}$	12
	Ca:Si = 1.0	2		12.1	$1\cdot10^{-6}$-$3\cdot10^{-3}$	8
	Ca:Si = 1.6	2		12.6	$1\cdot10^{-6}$-$2\cdot10^{-3}$	7
HCP, deg. stage II		2	4-145	12.7	$1\cdot10^{-6}$-$3\cdot10^{-3}$	7
Low pH cement (*CEBAMA ref. cement*)		2	60	11.4	$1\cdot10^{-6}$-$3\cdot10^{-3}$	7
TiO_2	p.w. C-S-H 1.0	2	1-20	12.1	$1\cdot10^{-5}$-$3\cdot10^{-4}$	4
	p.w. HCP deg. stage II	2		12.6	$1\cdot10^{-5}$-$3\cdot10^{-4}$	4
	p.w. HCP deg. stage I	2		13.2	$1\cdot10^{-5}$-$3\cdot10^{-4}$	4

Beryllium concentration and pH in each sample were monitored at regular time and 23 ± 2 °C intervals from 1-145 days until equilibrium conditions were attained. An aliquot of the supernatant (200 to 500 μL) of each sample was centrifuged for 2–3 minutes with 10 kD filters (2–3 nm cut-off Nanosep® centrifuge tubes, Pall Life Sciences) to separate colloids or suspended particles. After centrifugation, the respective volume of the filtrate was diluted (1:40 to 1:1000, depending upon initial Be concentration) in 2% ultrapure HNO_3, and [Be] was quantified by ICP–MS (inductively coupled plasma mass spectrometry, Perkin Elmer ELAN 6100). The accuracy of ICP–MS measurements was ± 2–5%. Detection limit varied between $10^{-5.5}$ and 10^{-8} M depending on the dilution factor. Previous tests experiments confirmed that the sorption of Be(II) in the 10 kD filters is not significant in the pH- and [Be]-range investigated in this study.

Before the addition of beryllium in each sample as well as after attaining the thermodynamic equilibrium in all investigated systems, the concentrations of Ca, K and Na were quantified using ICP-OES (inductively coupled plasma–optical emission spectroscopy, Perkin–Elmer 4300 DV) in order to determine the composition of the aqueous phase. The replicate aliquots taken from the supernatant (200 to 500 μL) were ultrafiltrated (2-3 minutes centrifugation with 10 kD filters) and diluted (1:40 to 1:100) in 2% HNO_3. The detection limit of this technique is $\approx 10^{-4}$ to $\approx 10^{-5}$ M, depending on the measured element and dilution factor.

Sorption kinetics were investigated following the evolution of the distribution ratio, R_d (in $L \cdot kg^{-1}$), as a function of time. R_d values were calculated as the ratio of beryllium concentration in the solid ($[Be]_{solid}$, in $mol \cdot kg^{-1}$) and aqueous ($[Be]_{aq}$, in M) phases:

$$R_d = \frac{[Be]_{sol}}{[Be]_{aq}} \cdot \frac{V}{m} = \frac{[Be]_0 - [Be]_{aq}}{[Be]_{aq}} \cdot \frac{V}{m} \quad (1)$$

where $[Be]_0$ is the initial beryllium concentration, V is the volume of sample (L) and m is the mass of the solid used as sorbent (kg).

The uptake of beryllium under equilibrium conditions *i.e.* after contact time of >125 days for cementitious phases was evaluated in terms of sorption isotherms ($\log [Be]_{solid}$ *vs.* $\log [Be]_{aq}$), although distribution ratios were also used to compare the uptake of Be(II) with other metal ions.

2.5. Computational methods

Molecular dynamics was used to study the sorption of beryllium on the C-S-H surface. Combinational analysis of the time-averaged local structures and 1D and 2D density profiles for target aqueous species provides an insight into the preferential sorption sites of Be(II) on the C-S-H surface.

Calculations were performed using the (001) surface of C-S-H. This is the most typical cleavage plane of C-S-H, parallel to silicate chains and CaO-layers, where the least number of bonds had to be broken. The model of this surface was taken from (Jamil et al. 2020). All the bridging Si were removed to get the structure of C-S-H with Ca:Si > 1.4 following available experimental spectroscopy data (Cong and Kirkpatrick 1996; Roosz et al. 2018). The silanol groups were deprotonated, and missing Si were replaced by Ca^{2+}. The deprotonated oxygen atoms of the surface were assigned a partial charge of $q_{onb} = -1.3|e|$, higher than the protonated ones in the standard ClayFF model (Androniuk et al. 2017; Kirkpatrick et al. 2005a; Kirkpatrick et al. 2005b).

The interfacial aqueous solution contained 6 ions of $Be(OH)_3^-$, and 4 $Be(OH)_4^{2-}$ with ~ 5400 H_2O molecules, which approximately corresponds to 0.1 M beryllium ion concentration and pH of ~ 12.7, as estimated using thermodynamic data reported in (Cevirim-Papaioannou et al. 2020). This relatively high concentration had to be used in the simulations for better statistical sampling. The possible formation of polynuclear Be-species under these conditions was also

evaluated in the calculations. Aqueous hydroxyl ions were added to the system in order to maintain the total electrostatic neutrality of the models.

Three-dimensional periodic boundary conditions (Allen and Tildesley 2017) were applied to the constructed model interface, and the thickness of the solution layer between the two external C-S-H surfaces was large enough (≈ 70 Å) to ensure that the interactions at the surfaces would not affect each other, and result in bulk-like solution behavior at distance d > 10 Å from each surface (Figure 1).

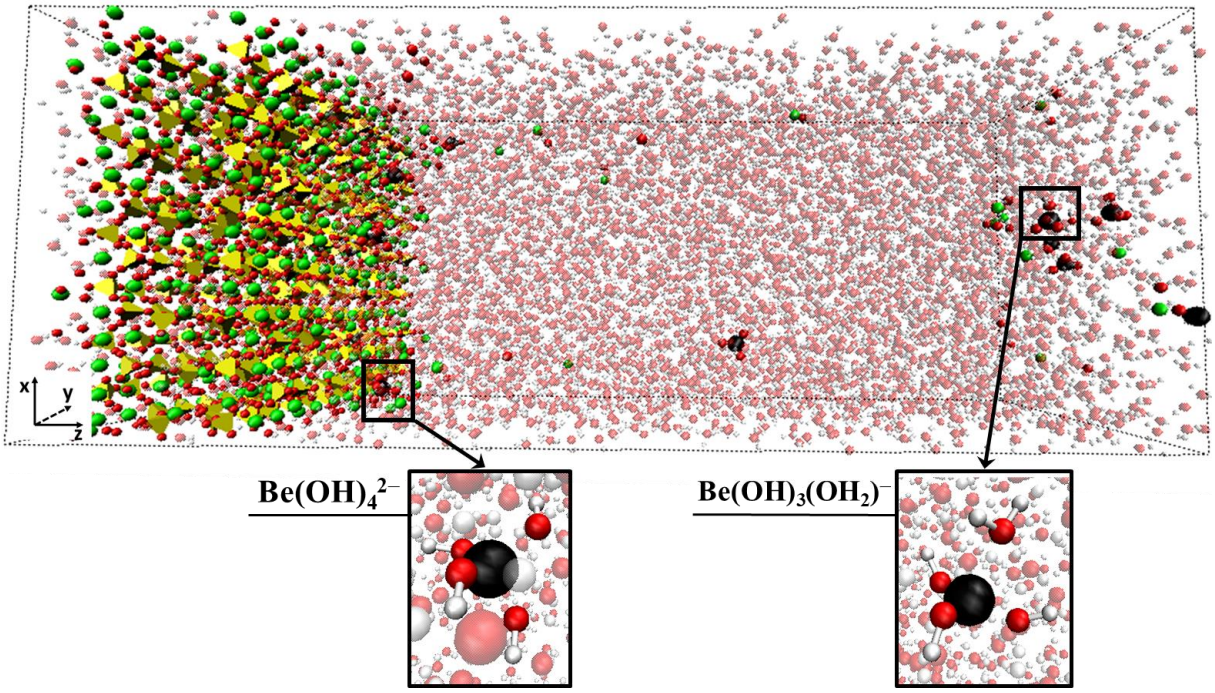

Figure 1. *Snapshot of (001) C-S-H simulation supercell. Colour scheme: Si – yellow; Ca – green; O – red; H – white; Be – black. Water molecules shown in transparent for clarity.*

The interatomic interaction parameters for C-S-H and H_2O were taken from the ClayFF (Cygan et al. 2004), and its later modifications for cement systems (Kalinichev et al. 2007; Kirkpatrick et al. 2005b; Mishra et al. 2017). The 12-6-4 Lennard-Jones type non-bonded parameters for Ca^{2+} and Be^{2+}, which include the contribution from the ion-induced dipole interaction, were taken from Li and Merz (Li and Merz 2014).

Standard Lorenz-Berthelot mixing rules (Allen and Tildesley 2017) were applied to calculate short-range Lennard-Jones interactions between the unlike atoms (with a cut-off distance of 14 Å). Long-range electrostatic forces were evaluated by means of the Ewald summation method. The Verlet leapfrog algorithm was used to integrate the equations of motion with a time step of 0.001 ps. The simulation model was initially equilibrated for 5 ns in the isobaric–isothermal

statistical ensemble (NPT), then for 5 ns in the canonical ensemble (NVT). Temperature and pressure were constrained using the Nose-Hoover thermostat and barostat (Allen and Tildesley 2017) at ambient conditions (T = 300 K, P = 0.1 MPa). The equilibration process was monitored by assessing the temperature, pressure, individual components of the potential energy of the system, density, and dimensions of the simulation box, in order to confirm that these parameters reach their equilibrium steady-state values on average (Braun et al. 2019). The main MD production run was performed for 5 ns (NVT-ensemble). All simulations were performed using the LAMMPS software package (Plimpton 1995). VMD software package has been used for visualisation (Humphrey et al. 1996).

The most probable sorption sites on the C-S-H surfaces can be found based on the calculation of one-dimensional atomic density maps in the direction perpendicular to the surface, and atomic density distributions parallel to the surface in the defined layer of solution. These profiles were calculated as time averages over the entire duration of the corresponding equilibrium production runs, and over two statistically independent solid/solution interfaces of the simulation box: both surfaces are characterized by the same amount of created structural defects and are interacting with the aqueous solution of the identical composition.

The local atomic density is calculated through the evaluation of the average number of atoms of a type A ($\bar{N}_A$) found within the range of distances from z to z+Δz parallel to the surface:

$$\text{Density}_A = \frac{\bar{N}_A(\Delta z)}{V_{cell}} \quad (2)$$

where V_{cell} is the total volume of the simulation cell, and Δz = 0.1 Å. The two-dimensional density in the xy plane within a layer of solution parallel to the surface at a certain distance z is defined by the probability of finding an atom of type A at a position (x,y) above the surface (Δx = Δy = 0.2 Å):

$$\text{Surface density}_A(x,y) = \bar{N}_A(\Delta x \Delta y) \quad (3)$$

3. Results and discussion

3.1. Characterization of the pore water solutions in equilibrium with cement and C-S-H phases

Table 2 summarizes the pore water composition (pH and concentrations of Na, K, Ca and Si) in contact with the investigated cement systems (C-S-H phases with Ca:Si = 0.6, 1.0 and 1.6, HCP in degradation stage II and low pH cement). These values are in line with data available in the literature for analogous systems (Atkins and Glasser 1992; Pointeau et al. 2004a; Tits et al. 2006b; Gaboreau et al. 2020; Tasi 2018; Ait-Mouheb 2021). As expected, C-S-H phases are characterized by an increase of pH and Ca concentration with increasing Ca:Si ratio. Similar pH and [Ca] are determined for C-S-H 1.6 and HCP in the degradation stage II, thus reflecting the predominance of C-S-H phases with high Ca:Si ratio in this degradation stage of cement. The values of pH and [Ca] in both systems are consistent with an equilibrium with portlandite.

Porewater compositions were also characterized after completing the sorption experiments with Be(II). Table SM-1 in the Supporting Material shows that no significant changes in the composition of the pore water occurred within the uptake process, except for the low pH cement equilibrated with the highest initial beryllium concentration ($[Be]_0 = 3.0 \cdot 10^{-3}$ M), for which a decrease of ≈ 0.3 pH-units was observed. These results support that the sorption process did not alter the composition of the sorbent material.

***Table 2**. Aqueous composition (pH, [Na], [K], [Ca], [Si]) of the pore water in contact with the investigated cement systems (C-S-H with Ca:Si = 0.6, 1.0, 1.6), HCP in the degradation stage II and low pH cement (CEBAMA reference cement). Measurements conducted after filtration and before the addition of Be(II) to the system. Pore water composition of the C-S-H phases was measured in two independent laboratories, BRGM (*) and KIT-INE ($^{\#}$).Related uncertainties are ± 0.1 for pH measurements and ± 2-30% for the measured concentrations.*

	pH	**Na [M]**	**K [M]**	**Ca [M]**	**[Si] [M]**
C-S-H 0.6	10.0 * / 10.0 $^{\#}$			$1.2\cdot10^{-3}$ * / $1.2\cdot10^{-3}$ $^{\#}$	$2.9\cdot10^{-3}$ *
C-S-H 1.0	12.0 * / 12.1 $^{\#}$			$4.0\cdot10^{-3}$ * / $4.6\cdot10^{-3}$ $^{\#}$	$3.4\cdot10^{-5}$ *
C-S-H 1.6	12.5 * / 12.6 $^{\#}$			$1.9\cdot10^{-2}$ * / $1.7\cdot10^{-2}$ $^{\#}$	$3.0\cdot10^{-6}$ *
HCP, deg. stage II	12.7	$1.0\cdot10^{-3}$	$8.6\cdot10^{-4}$	$2.0\cdot10^{-2}$	
Low pH cement (*CEBAMA reference cement*)	11.5	$1.8\cdot10^{-2}$	$7.3\cdot10^{-3}$	$7.5\cdot10^{-3}$	

3.2. Sorption kinetics

Figure 2 shows the sorption kinetics (as log R_d *vs.* time) for the uptake of Be(II) by C-S-H 1.6, HCP and TiO_2. A similar uptake behavior is observed for C-S-H 1.6 and HCP, thus highlighting the known analogies between these systems. In both cases, a fast sorption taking place within 4 days (log $R_d \approx 4.5$) is followed by a slower increase of the log R_d up to ≈ 5.5, with equilibrium conditions being attained at $t \geq 60$ days. This step-wise behavior expectedly reflects the involvement of two uptake mechanisms, possibly corresponding to a fast surface complexation process followed by the slower incorporation of Be(II) into the structure of C-S-H. A similar behavior has been previously described for other strongly sorbing metal ions, *e.g.* Zn(II), Nd(III), Eu(III), Np(IV) or U(VI) (Pointeau et al. 2001b; Ziegler et al. 2001a; Pointeau et al. 2004a; Schlegel et al. 2004; Stumpf et al. 2004; Mandaliev et al. 2010a; Mandaliev et al. 2010b; Tits et al. 2011; Gaona et al. 2011; Tits et al. 2015).

A much faster equilibrium ($t \geq 7$ days) is attained in the three investigated TiO_2 systems where no incorporation process is possible. TiO_2 is often considered as a model compound for the study of adsorption processes (Hakem et al. 1996; Guo et al. 2005; Bouby et al. 2010; Tits et al. 2014; Tits et al. 2015; Tits and Wieland 2018), and thus the fast uptake observed for Be(II) is exclusively attributed to surface complexation. Although showing similar uptake kinetics, significant differences arise for the adsorption of Be(II) onto TiO_2 at pH = 12.1 (log $R_d \approx 4.8$), 12.6 (log $R_d \approx 4.5$) and 13.2 (log $R_d \approx 2.5$). An extensive discussion of this observation is provided in Sections 3.4 and 3.5.

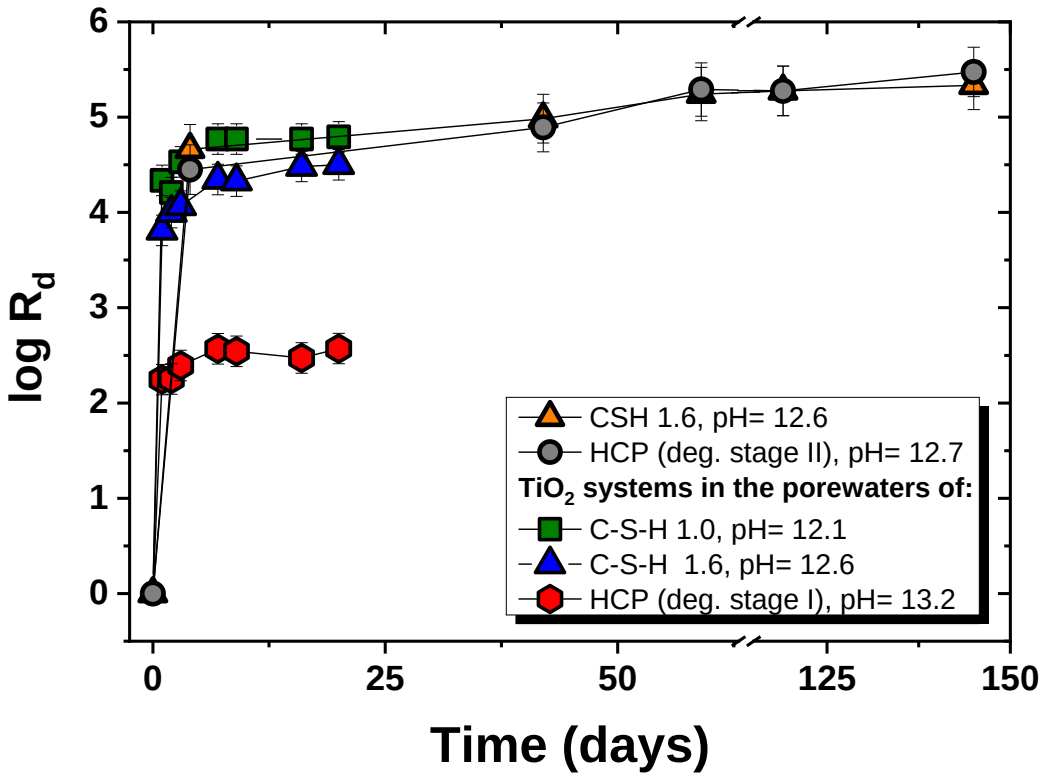

Figure 2. *Kinetics of the Be(II) uptake by C-S-H 1.6, HCP (degradation stage II) and TiO_2 (pore water solutions of C-S-H 1.0, 1.6 and HCP degradation stage I). Initial Be(II) concentrations are 10^{-4} M (C-S-H and HCP) and 10^{-4} M (TiO_2). R_d values expressed in L·kg^{-1}.*

3.3. Uptake of Be(II) by C-S-H, HCP (deg. stage II) and "low pH" cement: sorption isotherms

Sorption isotherms of Be(II) (as log $[Be]_{solid}$ *vs.* log $[Be]_{aq}$) for the uptake by C-S-H 1.0, C-S-H 1.6 and HCP (deg. stage II) are shown in Figure 3. The experimental window in the systems C-S-H 0.6 and low pH cement is limited by the low solubility of α-$Be(OH)_2$(s) at these pH values (≈ 10^{-7} to ≈ 10^{-6} M, see Cevirim-Papaioannou et al., 2020) and the detection limit of the ICP-MS technique (≈ 10^{-8} M). For this reason, insufficient data for the construction of the sorption isotherms were collected for these systems, and only log R_d values calculated on the basis of experiments with the lowest $[Be]_0$ are discussed in Section 3.5.

Figure 3 shows consistent Be(II) sorption data for the systems C-S-H 1.0, C-S-H 1.6 and HCP. All sorption isotherms show a linear trend over three orders of magnitude in $[Be]_{aq}$, in all cases with a slope of ≈ 1. This observation suggests that the same mechanism is controlling the uptake of beryllium under the investigated conditions. The grey regions in the figure illustrate the solubility limits of α-$Be(OH)_2$(cr) calculated at pH = 12.1 (light grey, C-S-H 1.0) and 12.6 (dark grey, C-S-H 1.6 and HCP) (Cevirim-Papaioannou et al. 2020). These regions define lower

solubility limits of Be(II) in the investigated conditions, bearing in mind that the formation of amorphous $Be(OH)_2$(am) expected in early precipitation stages may result in solubility limits 1-2 orders of magnitude higher. A slow decrease in the concentration of Be(II) is observed for the three samples in the dark grey region in Figure 3, corresponding to sorption experiments with $[Be]_0 = 10^{-2.5}$ and 10^{-3} M. These samples are considered to be controlled by solubility, with the slow decrease in concentration with time reflecting the transformation of the amorphous $Be(OH)_2$(am) into α-$Be(OH)_2$(cr) as reported in Cevirim-Papaioannou et al. (2020). Figure 3 shows also the sorption isotherms previously reported for the uptake of Sr(II) (C-S-H 1.07 and 1.6; Tits et al., 2006b), Zn(II) (C-S-H 1.0; Ziegler et al., 2001) and Th(IV) (HCP deg. stages I and II; Tits and Wieland, 2018). In spite of belonging to the same group in the periodic table, Sr(II) shows a much weaker and pH-dependent uptake compared to the Be(II) data obtained in the present study. These observations suggest that a different mechanism is controlling the uptake of both alkali-earth metals. Among all divalent ions, sorption isotherms reported for the uptake of Zn(II) by C-S-H (Ziegler et al. 2001a) show the closest behavior to the sorption data determined in the present study for Be(II). Although Ziegler and co-workers observed the precipitation of $CaZn_2(OH)_6{\cdot}2H_2O$(s) above log [Zn(II)] ≈ –4.2, the agreement with Be(II) sorption data is excellent down to [Zn(II)] ≈ –6. For the sake of comparison, Figure 3 includes also the sorption isotherms reported for a strongly sorbing metal, *i.e.* Th(IV). Tits and Wieland reported the sorption isotherms for the uptake of Th(IV) by HCP (deg. stages I and II) (Tits and Wieland 2018). The authors targeted very low metal concentrations (10^{-14}–10^{-7} M, using ^{228}Th) to avoid the precipitation of the sparingly soluble ThO_2(am, hyd). In spite of covering largely different metal concentrations, the overall uptake and the trend with increasing pH reported for Th(IV) by Tits and Wieland (2018) are similar to the results obtained in this study for Be(II). An extensive discussion on the uptake of Be(II) by C-S-H phases and cement in terms of log R_d values, as compared to other metal cations is provided in Section 3.5.

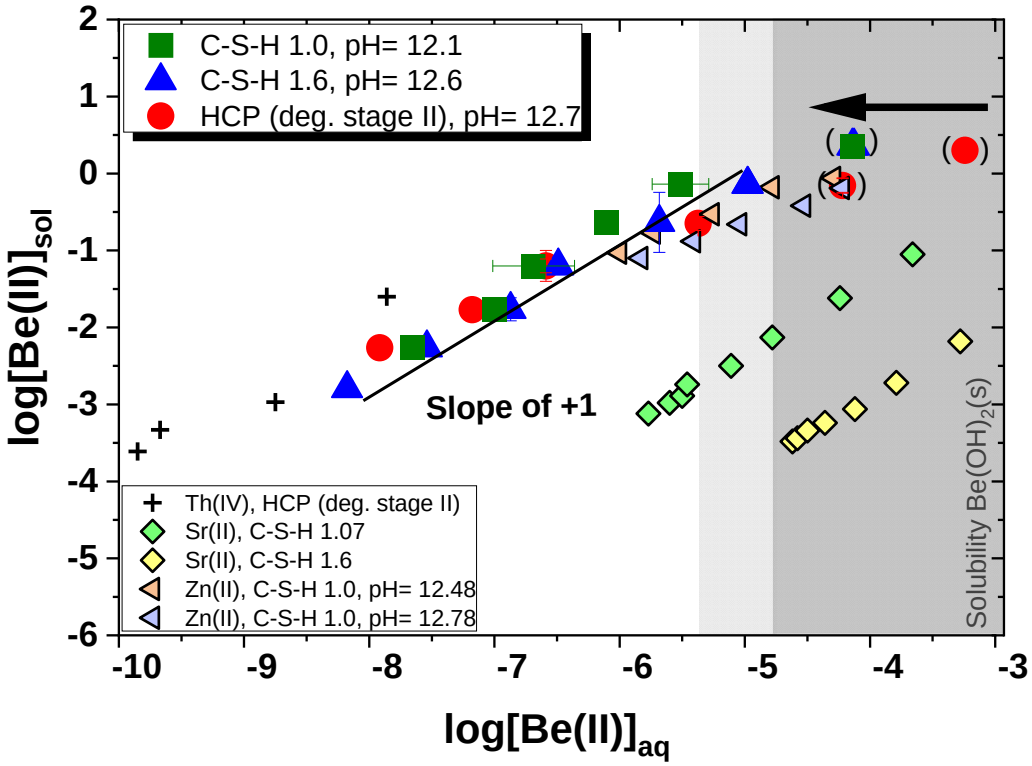

Figure 3. *Sorption isotherms of Be(II) taken up by C-S-H 1.0, 1.6 and HCP (deg. stage II). Grey regions correspond to the solubility limits of α-Be(OH)$_2$(cr) calculated at pH = 12.1 (light grey, C-S-H 1.0) and 12.6 (dark grey, C-S-H 1.6 and HCP) using thermodynamic data reported in Cevirim-Papaioannou et al. (2020). Sorption isotherms of Zn(II) (C-S-H 1.0 at pH= 12.48 and 12.78, Ziegler et al.,2001), Sr(II) (C-S-H 1.0 and 1.6, Tits et al., 2006) and Th(IV) (HCP deg. stage II, Tits and Wieland 2018) are appended for comparison.*

3.4. Uptake of Be(II) by TiO$_2$: sorption isotherms

Figure 4 shows the sorption isotherms for the uptake of Be(II) by TiO$_2$ in equilibrium with pore water solutions of C-S-H 1.0, C-S-H 1.6 and HCP (deg. stage I). In all cases, a linear sorption with slope ≈ +1 is observed. In contrast to C-S-H phases and HCP, the uptake of Be(II) by TiO$_2$ is strongly affected by pH, with a significant drop in log [Be]$_{solid}$ observed between pH = 12.1 and 13.2. These large differences can be partly explained by the different aqueous speciation of Be(II) at these pH values, with the predominance of $Be(OH)_3^-$ and $Be(OH)_4^{2-}$ at pH = 12.1 and 13.2, respectively, and assuming that the latter species does not sorb onto TiO$_2$. Based on the concept of electrostatic inter-ligand repulsion proposed by Neck *et al.* (2001) and the definition of limiting hydrolysis species for metal ions, Tits and co-workers elaborated on the uptake of highly hydrolyzed metal ions by TiO$_2$ in hyperalkaline pH conditions (10 ≤ pH ≤ 14) (Tits *et al.*, 2014). This approach was successfully applied to quantitatively explain the decrease in log

R_d values induced by the predominance of the limiting hydrolysis complexes $Np(V)O_2(OH)_2^-$ and $Np(VI)O_2(OH)_4^{2-}$ in the aqueous phase (with *n* hydroxo-groups), which accordingly hindered the step-wise formation of surface complexes with (*n* + 1) hydroxo- / oxo-groups. A similar effect could be claimed to explain the decreased uptake of Be(II) by TiO_2 in the pH-range where the limiting complex $Be(OH)_4^{2-}$ prevails.

The presence of Ca in hyperalkaline solutions has been reported to compensate the negative charge of the TiO_2 surface, and thus enhance the adsorption of negatively charged aqueous species (Tits et al., 2014). From the three investigated TiO_2 systems, the one in equilibrium with the pore water of HCP in the degradation stage I is characterized by the lowest Ca concentration ($7.5 \cdot 10^{-5}$ M), which possibly contributes to the weaker sorption observed for this system. The combination of both factors (pH and [Ca]) is considered to drive the large differences in the uptake of Be(II) by TiO_2 systems.

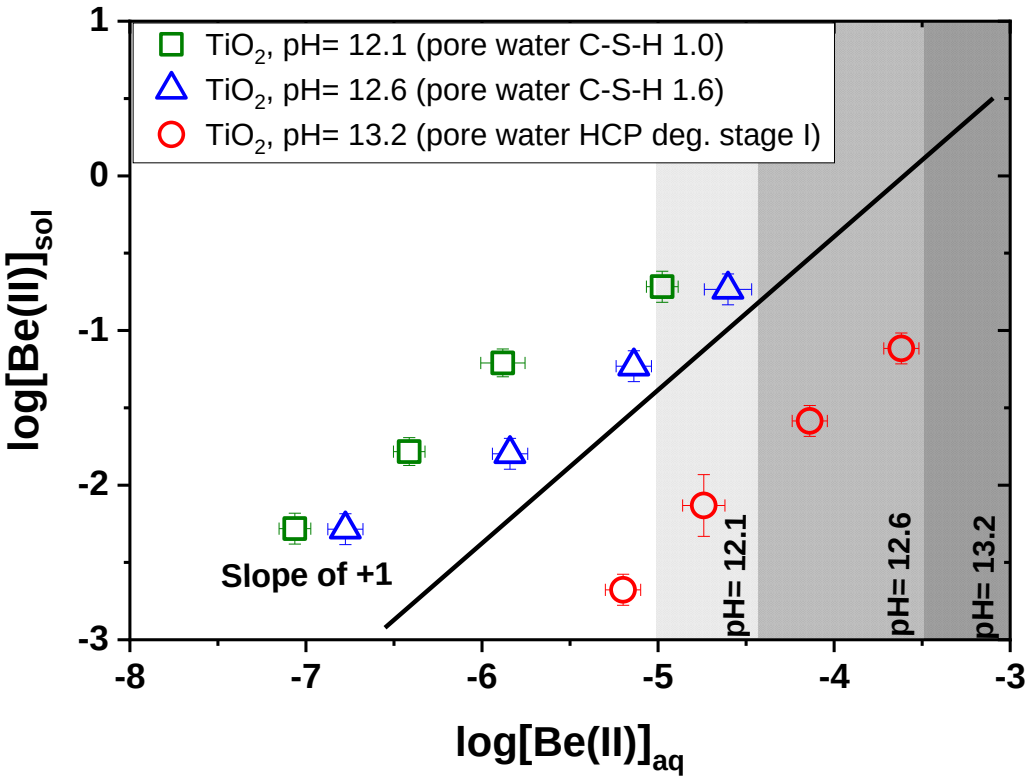

Figure 4. *Be Sorption isotherms of Be(II) taken up by TiO_2 equilibrated with pore water solutions of C-S-H 1.0, 1.6 and HCP (deg. stage I). Grey regions correspond to the solubility limits of α-$Be(OH)_2$(cr) calculated at pH = 12.1 (light grey, C-S-H 1.0), 12.6 (dark grey, C-S-H 1.6) and 13.2 (dashed grey, HCP deg. stage I) using thermodynamic data reported in Cevirim-Papaioannou et al. (2020).*

3.5. Discussion of log R_d values and comparison with other M(II)

Figure 5a summarizes the log R_d values of all investigated C-S-H, cement and TiO_2 systems. The figure includes also the log R_d value for the uptake of Be(II) by HCP in the degradation stage I as reported in Han *et al.* (2021). Dashed lines in the figure represent the highest distribution ratios (log $R_{d,max}$) that can be quantified for experiments at S/L = 0.2 and 2 $g \cdot L^{-1}$, considering a detection limit of $\approx 10^{-8}$ M. Very high log R_d values (5 – 7, with R_d in $L \cdot kg^{-1}$) are determined for all C-S-H and cement materials investigated. The strongest sorption (log $R_d \approx$ 7) is observed for the system C-S-H 0.6, which is characterized by the lowest pH conditions investigated in this study (pH ≈ 10). The uptake decreases to log $R_d \approx 6.1$ for low pH cement (pH ≈ 11.5), and further to log $R_d \approx 5$ for C-S-H 1.0 (pH ≈ 12.1). Above this pH, all investigated cement systems hold similar distribution ratios, with log $R_d \approx 5$. We hypothesize that the predominance of the neutral aqueous species $Be(OH)_2(aq)$ in the pore water of C-S-H 0.6 may be responsible for the stronger uptake observed for this system.

The log R_d values determined in this work for Be(II) are significantly higher than those reported for the uptake of other divalent cations by C-S-H and HCP, *i.e.* Sr(II) ($1 \leq \log R_d \leq 3.3$), Ba(II) ($1.3 \leq \log R_d \leq 3.7$), Ra(II) ($2 \leq \log R_d \leq 4.1$), Fe(II) (≈ 2) or Pb(II) ($2.9 \leq \log R_d \leq 3.8$), with the exception of Zn(II) ($4.3 \leq \log R_d \leq 5.5$) (Pointeau et al. 2001a; Ziegler et al. 2001a; Wieland and Van Loon 2003; Tits et al. 2006a; Tits et al. 2006b; Wieland et al. 2008; Wieland 2014; Missana et al. 2017; Olmeda et al. 2019; Mancini et al. 2020).

The large differences between log R_d values of M(II) possibly reflect the different mechanisms controlling the uptake of these metal cations by cementitious materials. The uptake of alkali-earth metals by C-S-H phases is driven by ion-exchange in the case of Sr(II) (Tits et al., 2006b), but is controlled by a combination of surface complexation and ion-exchange in the case of Ba(II) and Ra(II) (Tits et al. 2006a; Missana et al. 2017; Olmeda et al. 2019). Bernard and co-workers found no evidence for the uptake of Mg(II) by C-S-H phases, and instead reported the co-existence of two separate phases (C-S-H and M-S-H) within $10 \leq pH \leq 11$ (Bernard et al. 2018a; Bernard et al. 2018b).

Fe(II), Pb(II) and Zn(II) are characterized by the formation of anionic hydrolysis species in alkaline to hyperalkaline pH conditions. The solution chemistry of Fe(II) and Pb(II) is dominated by the species $M(OH)_3^-$ above pH ≈ 11-12 (Brown and Ekberg 2016; Bruno et al. 2018). Based on their XRD and EXAFS observations, Mancini and co-workers reported the presence of both surface- and interlayer-bound Fe(II) species in the sorption experiments with C-S-H phases (Mancini et al., 2020). In line with these observations, Pointeau et al. proposed

surface complexation as main mechanism for the uptake of Pb(II) by C-S-H (Pointeau et al., 2001).

In spite of their largely different ionic radii ($r_{Zn^{2+}}$ = 0.6 Å; $r_{Be^{2+}}$ = 0.27 Å; values corresponding to a CN = 4; Shannon, 1976), Zn(II) and Be(II) are characterized by a strong hydrolysis and the predominance of $M(OH)_3^-$ and $M(OH)_4^{2-}$ in hyperalkaline pH conditions (see Figures 5b and 5c). Zn(II) shows the strongest uptake by C-S-H of all previously reported divalent cations, with log R_d values slightly lower but comparable to Be(II). Based on their kinetic and spectroscopic (XAFS) data, Ziegler and co-workers reported a step-wise uptake of Zn(II) with a fast ($t \leq 4$ days) surface complexation process followed by the slower ($t \leq 87$ days) incorporation in the C-S-H interlayer (Ziegler et al., 2001a and 2001b). The similar kinetic behavior observed in this work for Be(II) possibly hints to analogous uptake mechanisms for both metal ions.

The values of log R_d determined in this work for Be(II) are also in line with data reported for strongly sorbing metal ions such as lanthanides or actinides in the +III and +IV oxidation states (Wieland and Van Loon 2003; Pointeau et al. 2004b; Wieland 2014; Tits and Wieland 2018; Haussler et al. 2018; Tasi 2018). The pH-independent behavior observed for the uptake of these elements by C-S-H and HCP can be partially explained by the invariant aqueous speciation within the pH-region covered by the different degradation stages of cement, *i.e.* Ln(III)/An(III)$(OH)_3$(aq) and An(IV)$(OH)_4$(aq). For the Ln(III)/An(III) systems, several spectroscopic studies (TRLFS, EXAFS) support their incorporation in the CaO-layer of C-S-H, which can be rationalized by the similar ionic radii of Ln^{3+}/An^{3+} and Ca^{2+}. In the case of An(IV), EXAFS studies hint to their incorporation in the interlayer of C-S-H (Gaona et al., 2011; Häussler et al., 2018).

The comparison of the uptake of Be(II) by C-S-H / HCP and TiO_2 in absolute terms is not straightforward due to the differences in the surface area of these materials (see Section 2.2). However, differences in the uptake trends observed for C-S-H / HCP and TiO_2 can be considered to gain indirect evidence on the mechanism controlling the uptake of Be(II) in cementitious systems. A significant decrease in the uptake is observed for TiO_2 systems between pH = 12.1 (log $R_d \approx 4.7$) and 13.2 (log $R_d \approx 2.5$). As discussed in Section 3.4, this trend is partly explained by the increasing fraction of the limiting complex $Be(OH)_4^{2-}$ in solution, which prevents the step-wise formation of the surface complex >S-O-$Be(OH)_4$. Within the same pH-region and boundary conditions, the uptake of Be(II) by C-S-H and HCP remains nearly constant at log $R_d \approx 5$. Together with the step-wise kinetic behavior, this observation is taken

as indirect evidence for the incorporation of Be(II) in the C-S-H structure, as opposed to the surface complexation mechanism reported to control the uptake of metal ions by TiO_2 (Bouby et al., 2010; Tits et al., 2011; Tits et al., 2014, among others).

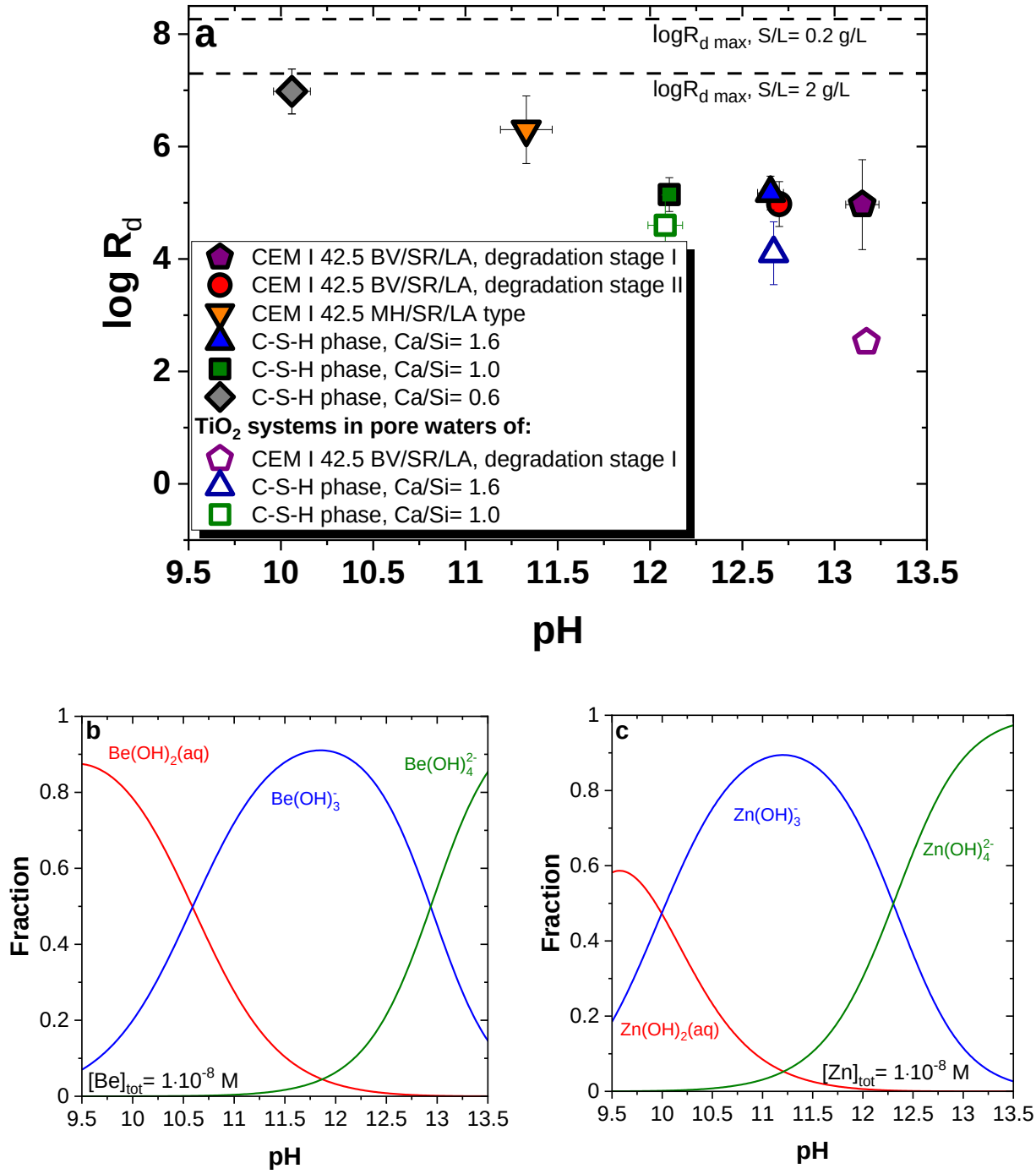

Figure 5. *(a) log R_d values determined in this work for the uptake of Be(II) by C-S-H (0.6, 1.0 and 1.6), HCP (deg. stage II), "low pH" cement and TiO_2. log R_d values reported in Han et al. (2021) for the uptake of Be(II) by HCP (deg. stage I) are appended for comparison. (b) Fraction diagrams of Be(II) and (c)Zn(II) calculated for $[M(II)]_{tot}= 1{\cdot}10^{-8}$ M and 9.5 ≤ pH ≤ 13.5) using thermodynamic data reported in Cevirim-Papaioannou et al. (2020) and Brown and Ekberg (2016), respectively.*

Wieland and Van Loon attempted to rationalize the uptake of metal ions by cement using the charge-to-size relationship (z/d) of the metal ion, where z is the charge of the metal ion and d is the M-O interatomic distance, with $d = r_{M^{z+}} + r_{O^{2-}}$. This relationship gives insight on the polarising effect of cations on anionic counter-ions (Wieland and Van Loon, 2003). As

highlighted by these authors, this approach explains the uptake on the basis of the ionic character of the bonding and irrespective of the underlying uptake mechanism, thus largely oversimplifying the uptake process. However, the approach appears useful to qualitatively explain the general trends observed for the uptake of metal ions by HCP, connecting the very strong sorption observed in this work for Be(II) with the uptake of apparently very different elements such as lanthanides or actinides. The original figure reported by Wieland and Van Loon for the uptake of Cs(I), Sr(II), Eu(III), Th(IV) and Sn(IV) by HCP (deg. stage I) has been extended in this work to Be(II) and other metal ions, including as well data for the uptake of these metals by HCP in the degradation stage II.

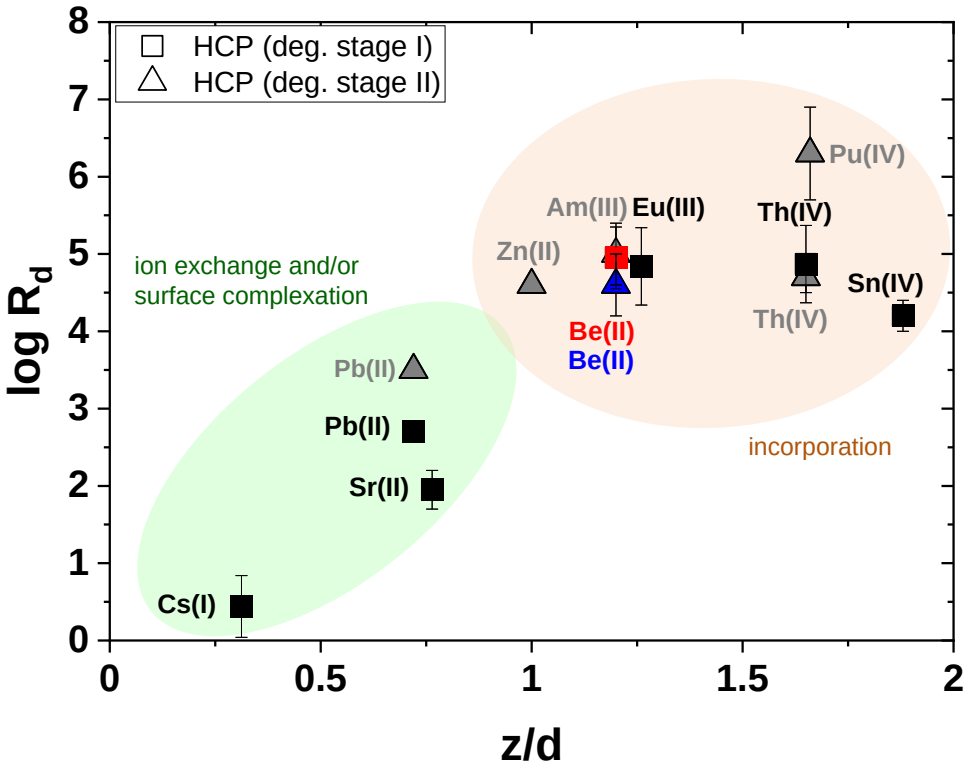

Figure 6. *Modification of the figure originally reported in Wieland and Van Loon (2003) for the uptake of different metal ions by HCP (deg. stage I) as a function of the charge-to-size relationship (z/d). The original figure has been updated with data for Be(II) (HCP in deg. stage II and I; this work; Han et al. 2021), Pb(II) (HCP deg. stage I and II; Wieland, 2014), Zn(II) (C-S-H at pH = 12.5; Ziegler et al., 2001), Am(III) (HCP deg. stage II; Pointeau et al., 2004); Th(IV) (HCP deg. stage II; Pointeau et al., 2004) and Pu(IV) (HCP deg. stage II; Tasi et al., 2021).*

Figure 6 shows two clear trends in the uptake of metal ions by HCP (deg. stages I and II). Lower log R_d values are obtained for metal ions with z/d < 1, which show also a clear tendency to decreasing log R_d with decreasing z/d. The uptake of these metals ions by cement and C-S-H phases has been predominantly reported as ion-exchange and / or surface complexation. Higher

and nearly constant log R_d values (log $R_d \approx 5 \pm 1$) are reported for those metal ions with $z/d \geq 1$. Spectroscopic evidences have systematically hinted to the incorporation in the C-S-H structure (*i.e.* CaO-layer or interlayer) as main uptake mechanism for the metal ions in this z/d region. We note the excellent agreement in the log R_d values determined in this work or reported in Han et al. (2021) for Be(II) (z/d = 1.20), with data reported for Eu(III) (z/d = 1.13) or Am(III) (z/d = 1.20). This exercise gives confidence in the incorporation of beryllium to the group of strongly sorbing metal ions in cementitious systems, usually restricted to lanthanides, actinides or highly charged cations (*e.g.* Sn^{4+} or Zr^{4+}).

3.6. Molecular dynamics simulation of the Be(II) uptake by C-S-H

The structural properties (coordination numbers and ion-ion distances) of hydrated beryllium ion in solution are reported in several theoretical and computational studies (Asthagiri and Pratt 2003; Raymond et al. 2020; Rozmanov et al. 2004; Rudolph et al. 2009). It is known that the Be^{2+} aqua complex has a preferred tetrahedral geometry, with an average Be-O_w distance of 1.64-1.67 Å (Azam et al. 2009; Smirnov and Trostin 2008). The calculated radial distribution functions and running coordination numbers for Be-O, Be-Ca, and Be-Be pairs in the studied interface can be found in Figure 7. Different kinds of oxygen atoms present in the system were treated separately: deprotonated (-Si-**O**$^-$), protonated (-Si-**O**H), and bridging (-Si-**O$_b$**-Si-) oxygens of silanol groups, water oxygens (O_w, **O**H_2), and oxygen of the aqueous hydroxyl ions (**O**H^-).

As it can be seen in Figure 7, hydroxyls are mostly bound to beryllium in the range of distances from 1.5 to 1.8 Å, while the water molecule in $Be(OH)_3(OH_2)^-$ is found at a longer distance (2.1-2.3 Å) because of the repulsion forces from the three neighbouring hydroxyl groups. A spontaneous proton transfer from the water molecule in the immediate coordination to the water molecule in the second coordination sphere is very probable (Azam et al. 2009), but this process cannot be modelled with classical MD. This proton transfer is not expected to affect the results of this study, since the process leads to the formation of $Be(OH)_4^{2-}$, which is also considered in the MD calculations.

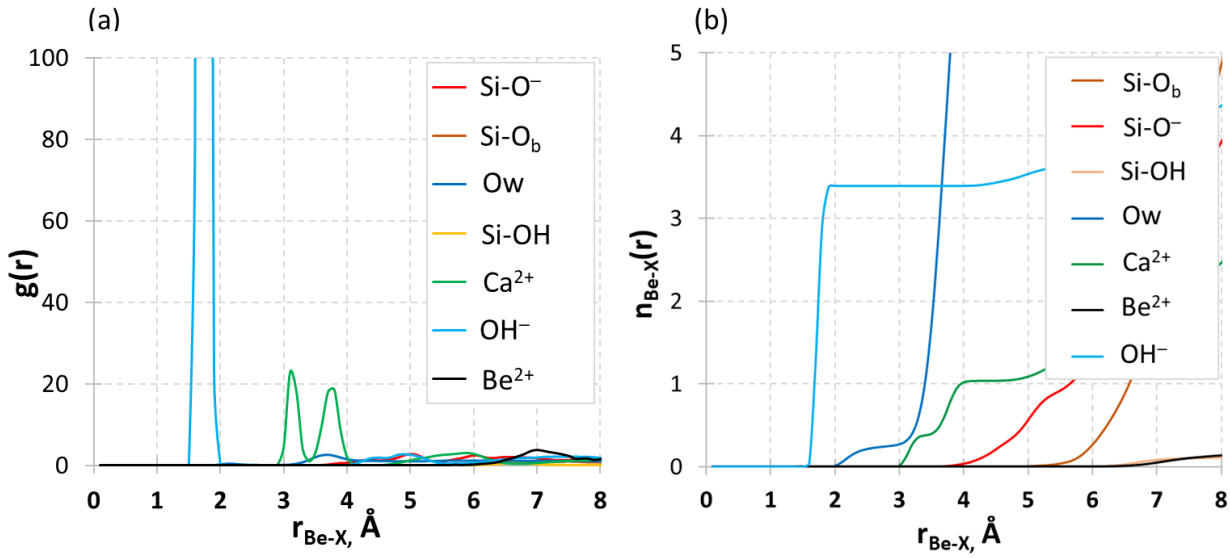

Figure 7. *(a) Radial distribution function and (b) running coordination numbers for Be^{2+} ion pairs.*

From the calculated running coordination numbers (*n*(r)) (Figure 7) it can be seen that beryllium hydroxo ions do not directly bind with silanol groups. It can be assumed, that the water molecule in $Be(OH)_3(OH_2)^-$ can be replaced by a deprotonated surface silanol group, but this was not possible in the given simulation time. As discussed in Section 3.2, the adsorption of Be(II) is not very fast, and the incorporation of Be^{2+} into the C-S-H structure is expected under equilibrium conditions. To be able to sample this kind of sorption, a different computational method will be used in the future to overcome the kinetic factor, *e.g.* umbrella sampling or replica MD. These calculations will consider also the C-S-H interlayer, which is expected to play a relevant role in the uptake of Be(II) and will be reported in a separate publication by Androniuk et al..

The probability peak of the deprotonated silanol group is found at $d > 4$ Å, which means that beryllium ions have approached the surface of C-S-H and stayed as stable bound complexes at the surface. Additionally, there is a strong interaction with Ca^{2+} cations: well-defined peaks can be found at the distances of 3.1 and 3.8 Å from Be^{2+}. These two distances correspond to Ca^{2+} coordination with Be^{2+} through 1 or 2 hydroxyl "bridges".

There is already experimental evidence that at high pH beryllium forms stable monomeric hydroxo complexes (Cevirim-Papaioannou et al. 2020). However, the probability of formation of polynuclear Be(II) species in the aqueous phase or on the interface was also assessed, as the hydroxo-bridges are common for beryllium in aqueous solutions (Alderighi et al. 2000).

Furthermore, the presence of a high concentration of Ca^{2+} counter ions can potentially induce the stabilization of $[Be_2(OH)_7]^{3-}$ anions (Schmidbaur 2001). The formation of Be(II) dimeric species was observed in bulk solution, but they were not stable over the production run. Furthermore, the running coordination number for the Be-Be pair does not show any significant peak, thus, formation and sorption of dimers were considered negligible within the investigated boundary conditions.

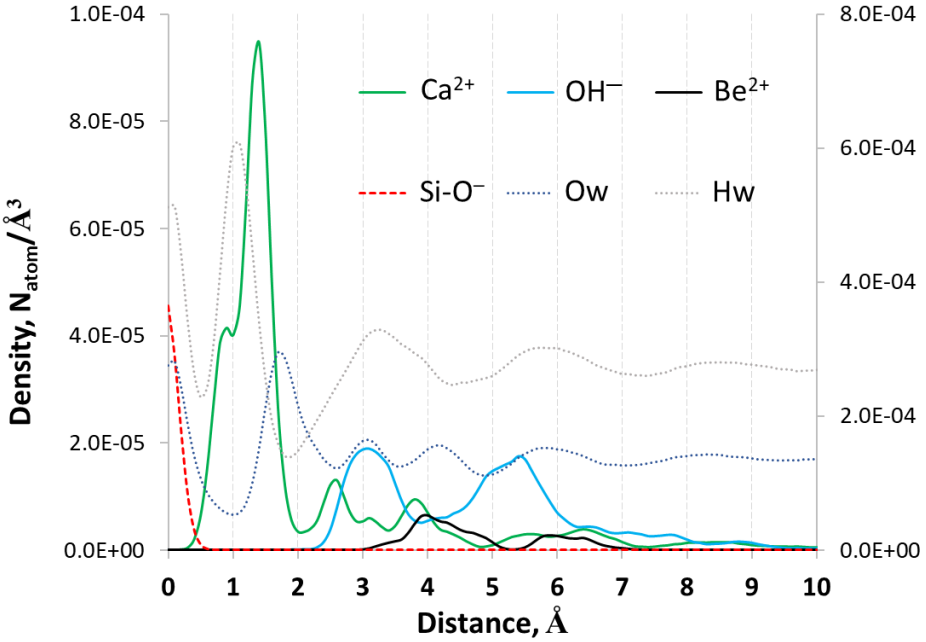

Figure 8. *Atomic density profiles of solution species near the C-S-H surface. The right-side axis shows densities plotted with dotted lines.*

Atomic density profiles next to the (001) surface of C-S-H are presented in Figure 8. As can be seen, at the distance > 8 Å there is no significant structuring of the interacting solution – it has a bulk-like behaviour.

It is well-known that Ca^{2+} is strongly attracted to the deprotonated negatively charged surface and forms a layer that at high Ca^{2+} concentration inverts the overall surface charge from negative to positive (Pointeau et al. 2006; Viallis-Terrisse et al. 2001). There are several possible binding geometries for Ca^{2+} with C-S-H silanol groups, therefore, a series of overlapped peaks of Ca^{2+} is found at a close distance from the surface. The highest peak at 1.5 Å corresponds to inner-sphere coordination with 2 silanol groups. Beryllium is found farther from the C-S-H surface, and the density profile is showing two distinct peaks: at the distance ranges of 3.0 – 5.2 Å and 5.3 – 7 Å. There is a maximum density of aqueous hydroxyl (OH^-) between adsorbed Ca^{2+} and Be^{2+} (2.5 – 3.5 Å). Partially these hydroxyls belong to Ca^{2+}-OH

pairs, and partially to Ca^{2+}- $Be(OH)_3^-$ and Ca^{2+}- $Be(OH)_4^{2-}$ adsorbed on the surface. As a result, the sorption of beryllium is observed not through the direct binding, but mostly through Ca-bridges (both coordination with surface Ca^{2+} and sorption of Ca-Be complexes from the solution is possible).

The formed complexes were stable during the production simulation time, which allowed us to identify them more accurately with the help of time-averaged *2D* surface maps. The contour density maps and the surface complexes of beryllium are shown in Figure 9.

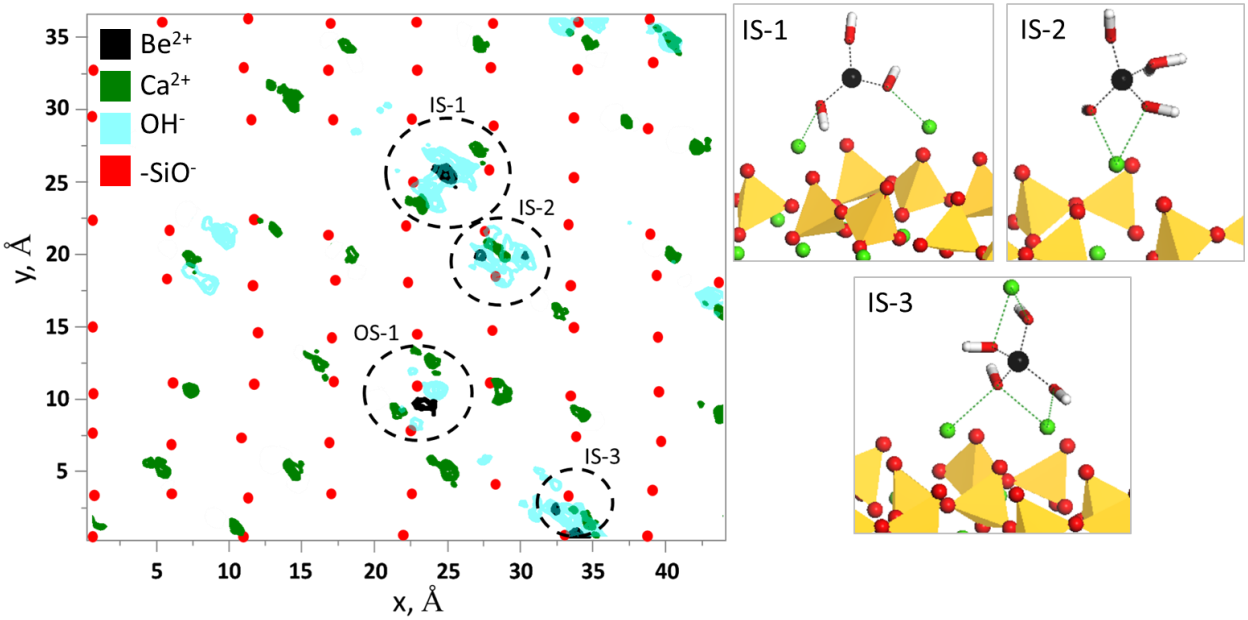

Figure 9. *Atomic density contour maps of time-averaged surface distributions of selected atoms at d ≈ 1-5 Å from the surface with the simulation snapshots of defined complexes (colour scheme: Si – yellow; Ca – green; O – red; H – white; Be – black).*

Beryllium is known to have a very ordered second coordination sphere. It was found that aqueous beryllium hydroxides can coordinate multiple Ca^{2+} cations of the C-S-H surface, forming potentially a much stronger surface complex. Three most stable inner-sphere (IS) complexes were identified: IS-1 ($Ca_2Be(OH)_3$ bound to 3 deprotonated silanol groups), IS-2 ($CaBe(OH)_3$ bound to 2 deprotonated silanol groups), and IS-3 ($Ca_3Be(OH)_4$ coordinated with 3 deprotonated silanol groups). These complexes correspond to the first beryllium maximum of the 1D density profile in Figure 9. Additionally, a stable outer-sphere complex (OS-1) was observed with water molecules present between Ca^{2+} and the surface that corresponds to the second maximum of the profile. Sorption of hydroxocomplexes on C-S-H through Ca bridging

has been already seen for uranyl (Androniuk et al., 2019), and this uptake mechanism could be expected for other divalent cations.

3.7. Conclusions

We have provided the first ever direct experimental evidence that Be(II) sorbs strongly in the cementitious systems investigated (HCP deg. stage II, low pH cement, C-S-H with Ca:Si = 0.6, 1.0 and 1.6). The similar uptake determined for cement and C-S-H phases confirms that the latter are the main sink of beryllium in cementitious materials. The kinetic behavior observed supports a two-step uptake mechanism, including a fast surface complexation process followed by the slower incorporation of Be(II) in C-S-H. The stronger uptake of Be(II) (log $R_d \approx 7$) observed at pH ≈ 10 correlates with the predominance of the neutral species $Be(OH)_2(aq)$ in solution. Lower and nearly constant log R_d values are determined within $12 \leq pH \leq 13.2$, suggesting a similar uptake of the anionic species $Be(OH)_3^-$ and $Be(OH)_4^{2-}$. In contrast to this finding, a clear decrease in log R_d values is observed for the uptake of Be(II) by TiO_2 within the same pH-range. This supports that incorporation is the main uptake mechanism in cement / C-S-H phases, as opposed to the surface complexation mechanism controlling the uptake of Be(II) by TiO_2.

Although the uptake of metal ions by cement and C-S-H phases is affected by several parameters (pH, metal speciation, [Ca], Ca:Si in the solid phase, etc.), it can be qualitatively explained by the charge-to-size ratio (z/d). This relationships satisfactorily explains the similar sorption observed for elements as different as Be(II) (z/d = 1.2), Zn(II) (z/d = 1.0), Eu(III) (z/d = 1.13) or Am(III) (z/d = 1.2) (Pointeau et al. 2004b; Wieland and Van Loon 2003; Ziegler et al. 2001a).

Molecular dynamics highlight the key role of Ca in the uptake of Be(II) by C-S-H phases. Three main surface complexes have been identified: $>Ca_2Be(OH)_3$ (bound to 3 deprotonated silanol groups), $>CaBe(OH)_3$ (bound to 2 deprotonated silanol groups), and $>Ca_3Be(OH)_4$ (coordinated with 3 deprotonated silanol groups). Molecular dynamics calculations have shown a great potential for the description of Be(II) uptake by the C-S-H surface, and future work at KIT-INE will target the description of processes taking place at the C-S-H interlayer, which is expected to play a relevant role in the uptake of Be(II) and other strongly sorbing metal ions.

This work provides a comprehensive quantitative and mechanistic description of the uptake of beryllium by cementitious material which so far was considered negligible in the view of lacking experimental studies. This new information is of high relevance and allows to better quantify the retention of beryllium in the context of the Safety Case for deep underground repositories for nuclear waste. It provides also a thorough scientific basis for the future development of more detailed thermodynamic / geochemical models, *e.g.* in the form of aqueous-solid solution models.

Acknowledgements

The research leading to these results has received funding from the European Union's European Atomic Energy Community's (Euratom) Horizon 2020 Programme (NFRP-2014/2015) under grant agreement, 662147 – Cebama. The research stay of S. Han at KIT–INE was partially funded through the Korea Nuclear International Cooperation Foundation (KONICOF) Nuclear Global Internship Program and the National Research Foundation of Korea funded by the Ministry of Education (NRF-2017M2B2B1072374).

Frank Geyer, Annika Kaufmann, Cornelia Walschburger and Melanie Böttle (all KIT–INE) are gratefully acknowledged for the ICP–MS/OES measurements and technical support. Thanks are due to Agost Gyula Tasi (KIT–INE) for his support with the preparation of the cement powder. Klas Källström (Swedish Nuclear Fuel and Waste Management Company, SKB) is kindly acknowledged for providing one of the cement rods used in this study. The authors wish to thank Francis Claret (BRGM) for his help with the exchange of C-S-H phases with KIT–INE.

References

Ait-Mouheb N. 2021 Radionuclides migration in the low-pH cement / clay interface. PhD thesis, University of Jena, Germany (in preparation)

Ait Mouheb N., Montoya V., Schild D., Soballa E., Adam C., Geyer F., Schäfer T. 2019 Characterization and sorption properties of low pH cements. In: Altmaier, M., Montoya, V., Valls A., *Proceeding of the Second workshop of the horizon 2020 CEBAMA project*, KIT scientific publishing, Karlsruhe, pp. 29-39.

Alderighi L., Gans P., Midollini S., Vacca A. 2000 Aqueous solution chemistry of beryllium. In: Sykes, A.G, Cowley, A. (Eds.), Main Chemistry Group, Advances in Inorganic Chemistry, Vol 50. Academic Press, San Diego, pp. 110-172.

Allen R., Tildesley D. J. 2017 Computer Simulation of Liquids. 2nd edition, Oxford University Press, New York, 99. 626.

Androniuk I., Kalinichev A. G. 2020 Molecular dynamics simulation of the interaction of uranium (VI) with the C-S-H phase of cement in the presence of gluconate. Appl. Geochem. 113. doi:10.1016/j.apgeochem.2019.104496

Androniuk I., Landesman C., Henocq P., Kalinichev A. G. 2017 Adsorption of gluconate and uranyl on C-S-H phases: Combination of wet chemistry experiments and molecular dynamics simulations for the binary systems. Phys. Chem. Earth 99:194-203. doi:10.1016/j.pce.2017.05.005

Asthagiri D., Pratt L. R. 2003 Quasi-chemical study of Be^{2+}(aq) speciation. Chem. Phys. Lett. 371 (5-6):613-619. doi:10.1016/S0009-2614(03)00227-6

Atkins M., Glasser F. P. (1992) Application of Portland cement-based materials to radioactive waste immobilization. Waste Manage.12 (2-3):105-131. doi:DOI 10.1007/s10582-003-0081-0

Atkinson A., Everitt N., Guppy R. 1988 Evolution of pH in a rad-waste repository: Internal reactions between concrete constituents. UKAEA Report, AERE-R12939, Harwell, UK.:100-113. doi:Doi 10.13182/Nt88-A34082

Azam S. S., Hofer T. S., Bhattacharjee A., Lim L. H. V., Pribil A. B., Randolf B. R., Rode B. M. 2009 Beryllium(II): The Strongest Structure-Forming Ion in Water? A QMCF MD Simulation Study. J. Phys. Chem. B 113 (27):9289-9295. doi:10.1021/jp903536k

Barzgar S., Lothenbach B., Tarik M., Di Giacomo A., Ludwig C. 2020 The effect of sodium hydroxide on Al uptake by calcium silicate hydrates (C-S-H). J. Colloid Interf. Sci. 572:246-256. doi:10.1016/j.jcis.2020.03.057

Bayliss S., Ewart F. T., Howse R. M., Lane S. A., Pilkington N. J., Smith-Briggs J. L., Willimams S. J. 1989 The solubility and sorption of radium and tin in a cementitious near-field environment. Mater. Res. Soc. Symp. Proc.127, 879-885.

Beeston J. M. 1970 Beryllium metal as a neutron moderator and reflector material. Nucl. Eng. Des. 14 (3):445

Bernard E., Dauzeres A., Lothenbach B. 2018a Magnesium and calcium silicate hydrates, Part II: Mg-exchange at the interface "low-pH" cement and magnesium environment studied in a C-S-H and M-S-H model system. Appl. Geochem. 89:210-218. doi:10.1016/j.apgeochem.2017.12.006

Bernard E., Lothenbach B., Cau-Dit-Coumes C., Chlique C., Dauzeres A., Pochard I. 2018b Magnesium and calcium silicate hydrates, Part I: Investigation of the possible magnesium incorporation in calcium silicate hydrate (C-S-H) and of the calcium in magnesium silicate hydrate (M-S-H). Appl. Geochem. 89:229-242. doi:10.1016/j.apgeochem.2017.12.005

Berner U. R. 1992 Evolution of porewater chemistry during degrardation of cement in a radioactive waste repository environment. Waste Manage. 12:201-219

Bouby M., Lutzenkirchen J., Dardenne K., Preocanin T., Denecke M. A., Klenze R., Geckeis H. 2010 Sorption of Eu(III) onto titanium dioxide: Measurements and modeling. J. Colloid Interf. Sci. 350 (2):551-561. doi:10.1016/j.jcis.2010.06.060

Braun E., Gilmer J., Mayes H. B., Mobley D. L., Monroe J. I., Prasad S., Zuckerman D. M., Datzmann T. 2019 Best Practices for Foundations in Molecular Simulations [Article v1.1]. Living J. Comp. Mol. Sci. 1 (1):5957. doi:10.11646/zootaxa.4563.3.8

Brown P. L., Ekberg C. 2016 Hydrolysis of Metal Ions, Wiley-VCH Verlag GmbH, Weinheim, Germany.

Bruno J., González-Siso M. R., Duro L., Gaona X., Altmaier M. 2018 Key master variables affecting the mobility of Ni, Pu, Tc and U in the near field of the SFR repository. Main experimental findings and PA implications of the PhD thesis, SKB tehcnical report, 18-01, Svensk Kärnbränslehantering AB, Solna, Sweden. doi:Doi 10.1039/Dt9870002439

Bu J., Teresa R. G., Brown K. G., Sanchez F. 2019 Adsorption mechanisms of cesium at calcium-silicate-hydrate surfaces using molecular dynamics simulations. J. Nucl. Mater. 515:35-51. doi:10.1016/j.jnucmat.2018.12.007

Calvo J. L. G., Hidalgo A., Alonso C., Luco L. F. 2010 Development of low-pH cementitious materials for HLRW repositories Resistance against ground waters aggression. Cement Concrete Res. 40 (8):1290-1297. doi:10.1016/j.cemconres.2009.11.008

Cevirim-Papaioannou N., Gaona X., Böttle M., Yalcintas Bethune E., Schild D., Adam C., Sittel T., Altmaier M. 2020 Thermodynamic description of Be(II) solubility and hydrolysis in acidic to hyperalkaline NaCl and KCl solutions. Appl. Geochem. 117:1-13

Chandler D., Primm R. T., Maldonado G. I. 2009 Reactivity Accountability Attributed to Beryllium Reflector Poisons in the High Flux Isotope Reactor , ORNL Report, TM-2009/188, Oak Ridge, USA.

Churakov S. V., Labbez C. 2017 Thermodynamics and Molecular Mechanism of Al Incorporation in Calcium Silicate Hydrates. J Phys Chem C 121 (8):4412-4419. doi:10.1021/acs.jpcc.6b12850

Codina M., Cau-Dit-Coumes C., Le Bescop P., Verdier J., Ollivier J. P. 2008 Design and characterization of low-heat and low-alkalinity cements. Cement Concrete Res. 38 (4):437-448. doi:10.1016/j.cemconres.2007.12.002

Cong X. D., Kirkpatrick R. J. 1996 Si-29 MAS NMR study of the structure of calcium silicate hydrate. Adv. Cem. Based Mater. 3 (3-4):144-156. doi:Doi 10.1016/S1065-7355(96)90046-2

Coumes C. C. D., Courtois S., Nectoux D., Leclercq S., Bourbon X. 2006 Formulating a low-alkalinity, high-resistance and low-heat concrete for radioactive waste repositories. Cement Concrete Res. 36 (12):2152-2163. doi:10.1016/j.cemconres.2006.10.005

Cygan R. T., Liang J. J., Kalinichev A. G. 2004 Molecular models of hydroxide, oxyhydroxide, and clay phases and the development of a general force field. J. Phys. Chem. B 108 (4):1255-1266. doi:10.1021/jp0363287

D'Incal A., Hofer T. S., Randolf B. R., Rode B. M. 2006 Be(II) in aqueous solution - an extended ab initio QM/MM MD study. Phys Chem Chem Phys 8 (24):2841-2847. doi:10.1039/b603222b

Dauzeres A., Le Bescop P., Sardini P., Coumes C. C. D. 2010 Physico-chemical investigation of clayey/cement-based materials interaction in the context of geological waste disposal: Experimental approach and results. Cement Concrete Res. 40 (8):1327-1340. doi:10.1016/j.cemconres.2010.03.015

De S., Sabu G., Zacharias M. 2020 Molecular mechanism of Be^{2+}-ion binding to HLA-DP2: tetrahedral coordination, conformational changes and multi-ion binding. Phys. Chem. Chem. Phys. 22 (2):799-810. doi:10.1039/c9cp05695e

Gaboreau S., Grangeon S., Claret F., Ihiawakrim D., Ersen O., Montouillout V., Maubec N., Roosz C., Henocq P., Carteret C. 2020 Hydration Properties and Interlayer Organization in Synthetic C-S-H. Langmuir 36 (32):9449-9464. doi:10.1021/acs.langmuir.0c01335

Gaona X., Dahn R., Tits J., Scheinost A. C., Wieland E. 2011 Uptake of Np(IV) by C-S-H Phases and Cement Paste: An EXAFS Study. Environ. Sci. Technol. 45 (20):8765-8771. doi:10.1021/es2012897

Gnanakaran S., Scott B., McCleskey T. M., Garcia A. E. 2008 Perturbation of local solvent structure by a small dication: A theoretical study on structural, vibrational, and reactive properties of beryllium ion in water. J Phys Chem B 112 (10):2958-2963. doi:10.1021/jp076001w

Grangeon S., Fernandez-Martinez A., Baronnet A., Marty N., Poulain A., Elkaim E., Roosz D., Gaboreau S., Henocq P., Claret F. 2017 Quantitative X-ray pair distribution function analysis of nanocrystalline calcium silicate hydrates: a contribution to the understanding of cement chemistry. J Appl Crystallogr 50:14-21. doi:10.1107/S1600576716017404

Guo Z. J., Niu L. J., Tao Z. Y. 2005 Sorption of Th(IV) ions onto TiO_2: Effects of contact time, ionic strength, thorium concentration and phosphate. J. Radioanal. Nucl. Ch. 266 (2):333-338

Hakem N., Fourest B., Guillaumont R., Marmier N. 1996 Sorption of iodine and cesium on some mineral oxide colloids. Radiochim. Acta 74:225-230

Haussler V., Amayri S., Beck A., Platte T., Stern T. A., Vitova T., Reich T. 2018 Uptake of actinides by calcium silicate hydrate (C-S-H) phases. Appl. Geochem. 98:426-434. doi:10.1016/j.apgeochem.2018.08.021

Holland T. R., Lee D. J. 1992 Radionuclide Getters in Cement. Cement Concrete Res. 22 (2-3):247-258. doi:Doi 10.1016/0008-8846(92)90063-2

Honorio T., Benboudjema F., Bore T., Ferhat M., Vourc'h E. 2019 The pore solution of cement-based materials: structure and dynamics of water and ions from molecular simulations. Phys Chem Chem Phys 21 (21):11111-11121. doi:10.1039/c9cp01577a

Humphrey W., Dalke A., Schulten K. 1996 VMD: Visual molecular dynamics. J Mol Graph Model 14 (1):33-38. doi:Doi 10.1016/0263-7855(96)00018-5

Jamil T., Javadi A., Heinz H. 2020 Mechanism of molecular interaction of acrylate-polyethylene glycol acrylate copolymers with calcium silicate hydrate surfaces. Green Chem. 22 (5):1577-1593. doi:10.1039/c9gc03287h

Jenni A., Mader U., Lerouge C., Gaboreau S., Schwyn B. 2014 In situ interaction between different concretes and Opalinus Clay. Phys. Chem. Earth 70-71:71-83. doi:10.1016/j.pce.2013.11.004

Kalinichev A. G., Wang J. W., Kirkpatrick R. J. 2007 Molecular dynamics modeling of the structure, dynamics and energetics of mineral-water interfaces: Application to cement materials. Cement Concrete Res. 37 (3):337-347. doi:10.1016/j.cemconres.2006.07.004

Kawamura H., Tanaka S., Ishitsuka E. 2004 Proceedings of the Sixth IEA International Workshop on Beryllium Technology for Fusion, Miyazaki, Japan.

Kirkpatrick R. J., Kalinichev A. G., Hou X., Struble L. 2005a Experimental and molecular dynamics modeling studies of interlayer swelling: water incorporation in kanemite and ASR gel. Mater. Struct. 38 (278):449-458. doi:10.1617/14344

Kirkpatrick R. J., Kalinichev A. G., Wang J. 2005b Molecular dynamics modelling of hydrated mineral interlayers and surfaces: structure and dynamics. Mineral Mag. 69 (3):289-308. doi:10.1180/0026461056930251

Kremleva A., Kruger S., Rosch N. 2020 Uranyl(VI) sorption in calcium silicate hydrate phases. A quantum chemical study of tobermorite models. Appl. Geochem. 113. doi:10.1016/j.apgeochem.2019.104463

L'Hopital E., Lothenbach B., Le Saout G., Kulik D., Scrivener K. 2015 Incorporation of aluminium in calcium-silicate-hydrates. Cement Concrete Res. 75:91-103. doi:10.1016/j.cemconres.2015.04.007

Lange S., Kowalski P. M., Psenicka M., Klinkenberg M., Rohmen S., Bosbach D., Deissmann G. 2018 Uptake of Ra-226 in cementitious systems: A complementary solution chemistry and atomistic simulation study. Appl Geochem 96:204-216. doi:10.1016/j.apgeochem.2018.06.015

Li P. F., Merz K. M. 2014 Taking into Account the Ion-Induced Dipole Interaction in the Nonbonded Model of Ions. J. Chem. Theory Comput. 10 (1):289-297. doi:10.1021/ct400751u

Li Z., Song L. F., Li P., Merz K. M., Jr. 2020 Systematic Parametrization of Divalent Metal Ions for the OPC3, OPC, TIP3P-FB, and TIP4P-FB Water Models. J Chem Theory Comput 16 (7):4429-4442. doi:10.1021/acs.jctc.0c00194

Longhurst G. R., Carboneau M. I., Mullen C. K., J.W. S. 2003 Challenges for disposal of irradiated beryllium. Proceedings of the 6th IEA Workshop on Beryllium Technology, Dec. 2-5, Mizayaki, Japan.

Lothenbach B., Le Saout G., Ben Haha M., Figi R., Wieland E. 2012 Hydration of a low-alkali CEM III/B-SiO_2 cement (LAC). Cement Concrete Res. 42 (2):410-423. doi:10.1016/j.cemconres.2011.11.008

Lothenbach B., Nied D., L'Hopital E., Achiedo G., Dauzeres A. 2015 Magnesium and calcium silicate hydrates. Cement Concrete Res. 77:60-68. doi:10.1016/j.cemconres.2015.06.007

Mancini A., Wiealnd E., Geng G., Lotenbach B., Wehrli B., Dähn R. 2020 Fe(II) interaction with cement phases: Method development, wet, chemical studies and X-ray absorption spectroscopy. J. Colloid Interf. Sci. (in press)

Mandaliev P., Dahn R., Tits J., Wehrli B., Wieland E. 2010a EXAFS study of Nd(III) uptake by amorphous calcium silicate hydrates (C-S-H). J Colloid Interf Sci 342 (1):1-7. doi:10.1016/j.jcis.2009.06.011

Mandaliev P., Wieland E., Dahn R., Tits J., Churakov S. V., Zaharko O. 2010b Mechanisms of Nd(III) uptake by 11 angstrom tobermorite and xonotlite. Appl. Geochem. 25 (6):763-777. doi:10.1016/j.apgeochem.2010.01.002

Mishra R. K., Mohamed A. K., Geissbuhler D., Manzano H., Jamil T., Shahsavari R., Kalinichev A. G., Galmarini S., Tao L., Heinz H., Pellenq R., van Duin A. C. T., Parker S. C., Flatt R. J., Bowen P. 2017 cemff: A force field database for cementitious materials including validations, applications and opportunities. Cement Concrete Res. 102:68-89. doi:10.1016/j.cemconres.2017.09.003

Missana T., Garcia-Gutierrez M., Mingarro M., Alonso U. 2017 Analysis of barium retention mechanisms on calcium silicate hydrate phases. Cement Concrete Res. 93:8-16. doi:10.1016/j.cemconres.2016.12.004

Monteiro P. J. M., Geng G. Q., Marchon D., Li J. Q., Alapati P., Kurtis K. E., Qomi M. J. A. 2019 Advances in characterizing and understanding the microstructure of cementitious materials. Cement Concrete Res. 124. doi:10.1016/j.cemconres.2019.105806

Mutisya S. M., de Almeida J. M., Miranda C. R. 2017 Molecular simulations of cement based materials: A comparison between first principles and classical force field calculations. Comp Mater Sci 138:392-402. doi:10.1016/j.commatsci.2017.07.009

Ochs M., Dirk M., Wang L. (2016) Radionuclide and Metal Sorption on Cement and Concrete, Springer, Switzerland.

Ochs M., Talerico C., Lothenbach B. 2002 Systematic trends and empirical modeling of lead uptake by cements and cement minerals. Mater. Res. Soc. Symp. Proc. 757:101. doi:10.1557/PROC-757-II10.1

Olmeda J., Missana T., Grandia F., Grive M., Garcia-Gutierrez M., Mingarro M., Alonso U., Colas E., Henocq P., Munier I., Robinet J. C. 2019 Radium retention by blended cement pastes and pure phases (C-S-H and C-A-S-H gels): Experimental assessment and modelling exercises. Appl. Geochem. 105:45-54. doi:10.1016/j.apgeochem.2019.04.004

Plimpton S. 1995 Fast Parallel Algorithms for Short-Range Molecular-Dynamics. J. Comput. Phys. 117 (1):1-19. doi:DOI 10.1006/jcph.1995.1039

Pointeau I., Landesman C., Giffaut E., Reiller P. 2004a Reproducibility of the uptake of U(VI) onto degraded cement pastes and calcium silicate hydrate phases. Radiochim. Acta 92 (9-11):645-650. doi:DOI 10.1524/ract.92.9.645.55008

Pointeau I., Landesman C., Giffaut E., Reiller P., Coreau N., Moisan C., Reiller P. 2004b Etude de la retention chimique des radionucléides Cs(I), Am(III), Zr(IV), Pu(IV), Nb(V), U(VI) et Tc(IV) par es matériaux cimentaires degradés. Rapport Technique RT DPC/SECR 03-037. CEA, Saclay, France. doi:DOI 10.1524/ract.92.9.645.55008

Pointeau I., Marmier N., Fromage F., Fedoroff M., Giffault E. 2001a Cesium and Lead uptake by CSH phases of hydrated cement. Material Research Society Symposium Proceedings 663, 105-113.

Pointeau I., Piriou B., Fedoroff M., Barthes M. G., Marmier N., Fromage F. 2001b Sorption mechanisms of Eu^{3+} on CSH phases of hydrated cements. J. Colloid Interf. Sci. 236 (2):252-259. doi:DOI 10.1006/jcis.2000.7411

Pointeau I., Reiller P., Mace N., Landesman C., Coreau N. 2006 Measurement and modeling of the surface potential evolution of hydrated cement pastes as a function of degradation. J Colloid Interf Sci 300 (1):33-44. doi:10.1016/j.jcis.2006.03.018

Pomies M. P., Lequeux N., Boch P. 2001 Speciation of cadmium in cement Part I. Cd^{2+} uptake by C-S-H. Cement Concrete Res. 31 (4):563-569. doi:Doi 10.1016/S0008-8846(00)00480-4

Raymond O., Buhl M., Lane J. R., Henderson W., Brothers P. J., Plieger P. G. 2020 Ab Initio Molecular Dynamics Investigation of Beryllium Complexes. Inorg. Chem. 59 (4):2413-2425. doi:10.1021/acs.inorgchem.9b03309

Roosz C., Vieillard P., Blanc P., Gaboreau S., Gailhanou H., Braithwaite D., Montouillout V., Denoyel R., Henocq P., Made B. 2018 Thermodynamic properties of C-S-H, C-A-S-H and M-S-H phases: Results from direct measurements and predictive modelling. Appl. Geochem. 92:140-156. doi:10.1016/j.apgeochem.2018.03.004

Rozmanov D. A., Sizova O. V., Burkov K. A. 2004 Ab initio studies of the beryllium aquahydroxocomplexes. J. Mol. Struc-Theochem. 712 (1-3):123-130. doi:10.1016/j.theochem.2004.10.011

Rudolph W. W., Fischer D., Irmer G., Pye C. C. 2009 Hydration of beryllium(II) in aqueous solutions of common inorganic salts. A combined vibrational spectroscopic and ab initio molecular orbital study. Dalton T. (33):6513-6527. doi:10.1039/b902481f

Savage D., Benbow S. J. 2007 Low pH cements, SKI report, 2007:32, Swedish Nuclear Power Inspectorate, Stockholm, Sweden.

Schlegel M. L., Pointeau I., Coreau N., Reiller P. 2004 Mechanism of europium retention by calcium silicate hydrates: An EXAFS study. Environ. Sci. Technol. 38 (16):4423-4431. doi:10.1021/es0498989

Schmidbaur H. 2001 Recent contributions to the aqueous coordination chemistry of beryllium. Coordin. Chem. Rev. 215:223-241. doi:Doi 10.1016/S0010-8545(00)00406-9

Schmidt J., Vogelsberger W. 2009 Aqueous Long-Term Solubility of Titania Nanoparticles and Titanium(IV) Hydrolysis in a Sodium Chloride System Studied by Adsorptive Stripping Voltammetry. J. Solution. Chem. 38 (10):1267-1282. doi:10.1007/s10953-009-9445-9

Smirnov P. R., Trostin V. N. 2008 Structural Parameters of Hydration of Be^{2+} and Mg^{2+} Ions in Aqueous Solutions of Their Salts. Russ. J. Gen. Chem. 78 (9):1643-1649. doi:10.1134/S1070363208090016

Stumpf T., Tits J., Walther C., Wieland E., Fanghanel T. 2004 Uptake of trivalent actinides (curium(III)) by hardened cement paste: a time-resolved laser fluorescence spectroscopy study. J. Colloid Interf. Sci. 276 (1):118-124. doi:10.1016/j.jcis.2004.03.014

Tasi A. 2018 Solubility, redox and sorption behavior of plutonium in the presence of α-D-isosaccharinich acid cement under reducing conditions. PhD thesis, Karlsruhe Institute for Technology, Germany

Taylor H. F. W. 1997 Cement Chemistry, second ed. Thomas Telford, London.

Tits J., Gaona X., Laube A., Wieland E. 2014 Influence of the redox state on the neptunium sorption under alkaline conditions: Batch sorption studies on titanium dioxide and calcium silicate hydrates. Radiochim. Acta 102 (5):385-400. doi:10.1515/ract-2013-2151

Tits J., Geipel G., Mace N., Eilzer M., Wieland E. 2011 Determination of uranium(VI) sorbed species in calcium silicate hydrate phases: A laser-induced luminescence spectroscopy and batch sorption study. J. Colloid Interf. Sci. 359 (1):248-256. doi:10.1016/j.jcis.2011.03.046

Tits J., Iijima K., Wieland E., Kamei G. 2006a The uptake of radium by calcium silicate hydrates and hardened cement paste. Radiochim. Acta 94 (9-11):637-643. doi:10.1524/ract.2006.94.9.637

Tits J., Walther C., Stumpf T., Mace N., Wieland E. 2015 A luminescence line-narrowing spectroscopic study of the uranium(VI) interaction with cementitious materials and titanium dioxide. Dalton T. 44 (3):966-976. doi:10.1039/c4dt02172j

Tits J., Wieland E. 2018 Actinide sorption by cementitious materials, PSI technical report, 18-02, Paul Schwerer Institute, Villigen, Switzerland.

Tits J., Wieland E., Muller C. J., Landesman C., Bradbury M. H. 2006b Strontium binding by calcium silicate hydrates. J. Colloid Interf. Sci. 300 (1):78-87. doi:10.1016/j.jcis.2006.03.043

Tommaseo C. E., Kersten M. 2002 Aqueous solubility diagrams for cementitious waste stabilization systems. 3. Mechanism of zinc immobilization by calcium silicate hydrate. Environ. Sci. Technol. 36 (13):2919-2925. doi:10.1021/es0102484

Vasconcelos R. G. W., Walkley B., Day S., Tang C. C., Paraskevoulakos H., Gardner L. J., Corkhill C. L. 2020 18-month hydration of a low-pH cement for geological disposal of radioactive waste: The Cebama reference cement. Appl. Geochem. (in print)

Vehmas T., Montoya V., Alonso M. C., Vasicek R., Rastrick E., Gaboreau S., Vecernik P., Leivo M., Holt E., Fink N., Mouheb N. A., Svoboda J., Read D., Cervinka R., Vasconcelos R., Corkhill C. 2020 Characterization of Cebama low-pH reference concrete and assessment of its alteration with representative waters in radioactive waste repositories. Appl. Geochem. 121. doi:10.1016/j.apgeochem.2020.104703

Viallis-Terrisse H., Nonat A., Petit J. C. 2001 Zeta-potential study of calcium silicate hydrates interacting with alkaline cations. J. Colloid Interf. Sci. 244 (1):58-65. doi:DOI 10.1006/jcis.2001.7897

Wieland E. (2014) Sorption Data Base for the Cementitious Near Field of L/ILW and ILW Repositories for Provisional Safety Analyses for SGT-E2, Nagra Technical Report 14-08, Paul Scherrer Institut, Villigen, Switzerland. doi:DOI 10.1007/s10582-003-0081-0

Wieland E., Tits J., Kunz D., Daehn R. 2008 Strontium uptake by cementitious materials. Environ. Sci. Technol. 42 (2):403-409. doi:10.1021/es071227y

Wieland E., Van Loon L. (2003) Cementitious Near-Field Sorption Data Base for Performance Assessment of an ILW Repository in Opalinus Clay. Tehcnical report 03-06, Paul Scherrer Institut, Villigen, Switzerland. doi:DOI 10.1007/s10582-003-0081-0

Ziegler F., Giere R., Johnson C. A. 2001a Sorption mechanisms of zinc to calcium silicate hydrate: Sorption and microscopic investigations. Environ. Sci. Technol. 35 (22):4556-4561. doi:10.1021/es001768m

Ziegler F., Scheidegger A. M., Johnson C. A., Dahn R., Wieland E. 2001b Sorption mechanisms of zinc to calcium silicate hydrate: X-ray absorption fine structure (XAFS) investigation. Environ. Sci. Technol. 35 (7):1550-1555. doi:10.1021/es001437+

Supplementary Information

Table SI-1*. Aqueous composition (pH, [Na], [K], [Ca]) of the pore water in equilibrium with the investigated cement systems (C-S-H with Ca:Si = 1.0, 1.6), HCP in the degradation stage II and low pH cement (CEBAMA reference cement). Measurements conducted before and after the addition of Be(II) to the system. Related uncertainties are ± 0.1 for pH measurements and ±0.5-30% for the metal concentrations.*

		$[Be]_0$ [M]	pH	Na	K	Ca
C-S-H 1.0	**Absence of Be**		12.1			$4.6 \cdot 10^{-3}$
	Presence of Be	$1.0 \cdot 10^{-6}$	12.1			$4.8 \cdot 10^{-3}$
		$3.0 \cdot 10^{-6}$	12.1			$4.8 \cdot 10^{-3}$
		$1.0 \cdot 10^{-5}$	12.1			$4.8 \cdot 10^{-3}$
		$1.0 \cdot 10^{-4}$	12.1			$4.6 \cdot 10^{-3}$
		$3.0 \cdot 10^{-4}$	12.1			$4.6 \cdot 10^{-3}$
		$1.0 \cdot 10^{-3}$	12.1			$4.9 \cdot 10^{-3}$
		$3.0 \cdot 10^{-3}$	12.1			$4.4 \cdot 10^{-3}$
C-S-H 1.6	**Absence of Be**		12.7			$1.7 \cdot 10^{-2}$
	Presence of Be	$1.0 \cdot 10^{-6}$	12.7			$1.7 \cdot 10^{-2}$
		$3.0 \cdot 10^{-6}$	12.7			$1.6 \cdot 10^{-2}$
		$1.0 \cdot 10^{-5}$	12.7			$1.7 \cdot 10^{-2}$
		$3.0 \cdot 10^{-5}$	12.7			$1.7 \cdot 10^{-2}$
		$1.0 \cdot 10^{-4}$	12.7			$1.7 \cdot 10^{-2}$
		$3.0 \cdot 10^{-4}$	12.6			$1.7 \cdot 10^{-2}$
		$1.0 \cdot 10^{-3}$	12.6			$1.7 \cdot 10^{-2}$
		$3.0 \cdot 10^{-3}$	12.5			$1.7 \cdot 10^{-2}$
HCP II	**Absence of Be**		12.7	$1.0 \cdot 10^{-3}$	$8.6 \cdot 10^{-4}$	$2.0 \cdot 10^{-2}$
	Presence of Be	$1.0 \cdot 10^{-6}$	12.7	$2.6 \cdot 10^{-3}$	$7.0 \cdot 10^{-4}$	$2.1 \cdot 10^{-2}$
		$3.0 \cdot 10^{-6}$	12.7	$2.4 \cdot 10^{-3}$	$6.8 \cdot 10^{-4}$	$1.9 \cdot 10^{-2}$
		$1.0 \cdot 10^{-5}$	12.7	$1.7 \cdot 10^{-3}$	$5.8 \cdot 10^{-4}$	$1.9 \cdot 10^{-2}$
		$3.0 \cdot 10^{-5}$	12.7	$2.7 \cdot 10^{-3}$	$8.3 \cdot 10^{-4}$	$2.0 \cdot 10^{-2}$
		$1.0 \cdot 10^{-4}$	12.7	$2.4 \cdot 10^{-3}$	$7.0 \cdot 10^{-4}$	$2.0 \cdot 10^{-2}$
		$3.0 \cdot 10^{-4}$	12.7	$2.3 \cdot 10^{-3}$	$7.0 \cdot 10^{-4}$	$2.0 \cdot 10^{-2}$
		$1.0 \cdot 10^{-3}$	12.7	$2.3 \cdot 10^{-3}$	$7.0 \cdot 10^{-4}$	$2.0 \cdot 10^{-2}$
		$3.0 \cdot 10^{-3}$	12.6	$2.4 \cdot 10^{-3}$	$7.3 \cdot 10^{-4}$	$2.0 \cdot 10^{-2}$
Low pH cement	**Absence of Be**		11.47	$1.8 \cdot 10^{-2}$	$7.3 \cdot 10^{-3}$	$7.5 \cdot 10^{-3}$
	Presence of Be	$1.0 \cdot 10^{-6}$	11.36	$2.1 \cdot 10^{-2}$	$7.6 \cdot 10^{-3}$	$6.9 \cdot 10^{-3}$
		$1.0 \cdot 10^{-5}$	11.39	$2.0 \cdot 10^{-2}$	$7.5 \cdot 10^{-3}$	$6.9 \cdot 10^{-3}$
		$1.0 \cdot 10^{-4}$	11.39	$2.2 \cdot 10^{-2}$	$7.8 \cdot 10^{-3}$	$6.8 \cdot 10^{-3}$
		$3.0 \cdot 10^{-3}$	11.00	$2.1 \cdot 10^{-2}$	$7.7 \cdot 10^{-3}$	$7.7 \cdot 10^{-3}$